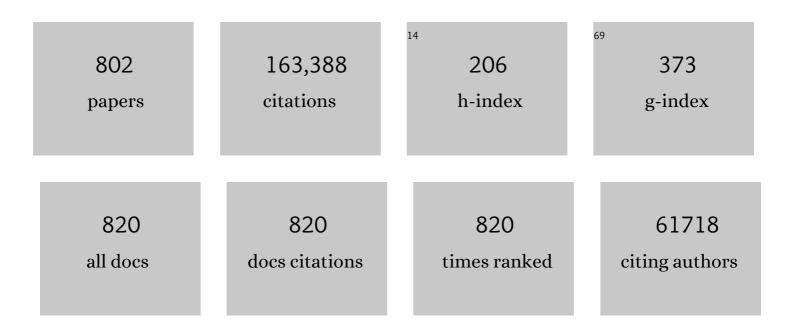
## List of Publications by Year in descending order

Source: https://exaly.com/author-pdf/2688127/publications.pdf Version: 2024-02-01



Ιμομο Υμ

#	Article	IF	CITATIONS
1	Heterojunction Photocatalysts. Advanced Materials, 2017, 29, 1601694.	21.0	3,143
2	Polymeric Photocatalysts Based on Graphitic Carbon Nitride. Advanced Materials, 2015, 27, 2150-2176.	21.0	3,046
3	Graphene-based semiconductor photocatalysts. Chemical Society Reviews, 2012, 41, 782-796.	38.1	2,497
4	Highly Efficient Visible-Light-Driven Photocatalytic Hydrogen Production of CdS-Cluster-Decorated Graphene Nanosheets. Journal of the American Chemical Society, 2011, 133, 10878-10884.	13.7	2,260
5	Synergetic Effect of MoS <sub>2</sub> and Graphene as Cocatalysts for Enhanced Photocatalytic H <sub>2</sub> Production Activity of TiO <sub>2</sub> Nanoparticles. Journal of the American Chemical Society, 2012, 134, 6575-6578.	13.7	2,245
6	Earth-abundant cocatalysts for semiconductor-based photocatalytic water splitting. Chemical Society Reviews, 2014, 43, 7787-7812.	38.1	2,125
7	S-Scheme Heterojunction Photocatalyst. CheM, 2020, 6, 1543-1559.	11.7	1,993
8	Allâ€5olidâ€5tate Zâ€5cheme Photocatalytic Systems. Advanced Materials, 2014, 26, 4920-4935.	21.0	1,989
9	Ultrathin 2D/2D WO3/g-C3N4 step-scheme H2-production photocatalyst. Applied Catalysis B: Environmental, 2019, 243, 556-565.	20.2	1,895
10	g <sub>3</sub> N <sub>4</sub> â€Based Heterostructured Photocatalysts. Advanced Energy Materials, 2018, 8, 1701503.	19.5	1,870
11	Enhanced Photocatalytic CO <sub>2</sub> -Reduction Activity of Anatase TiO <sub>2</sub> by Coexposed {001} and {101} Facets. Journal of the American Chemical Society, 2014, 136, 8839-8842.	13.7	1,701
12	Preparation and Enhanced Visible-Light Photocatalytic H <sub>2</sub> -Production Activity of Graphene/C <sub>3</sub> N <sub>4</sub> Composites. Journal of Physical Chemistry C, 2011, 115, 7355-7363.	3.1	1,694
13	Engineering heterogeneous semiconductors for solar water splitting. Journal of Materials Chemistry A, 2015, 3, 2485-2534.	10.3	1,609
14	Cocatalysts for Selective Photoreduction of CO <sub>2</sub> into Solar Fuels. Chemical Reviews, 2019, 119, 3962-4179.	47.7	1,591
15	Hierarchical photocatalysts. Chemical Society Reviews, 2016, 45, 2603-2636.	38.1	1,517
16	Enhanced photocatalytic performance of direct Z-scheme g-C3N4–TiO2 photocatalysts for the decomposition of formaldehyde in air. Physical Chemistry Chemical Physics, 2013, 15, 16883.	2.8	1,167
17	2D/2D Heterojunction of Ultrathin MXene/Bi <sub>2</sub> WO <sub>6</sub> Nanosheets for Improved Photocatalytic CO <sub>2</sub> Reduction. Advanced Functional Materials, 2018, 28, 1800136.	14.9	1,157
18	Direct Z-scheme photocatalysts: Principles, synthesis, and applications. Materials Today, 2018, 21, 1042-1063.	14.2	1,134

#	Article	IF	CITATIONS
19	The Effect of Calcination Temperature on the Surface Microstructure and Photocatalytic Activity of TiO2 Thin Films Prepared by Liquid Phase Deposition. Journal of Physical Chemistry B, 2003, 107, 13871-13879.	2.6	1,113
20	g-C <sub>3</sub> N <sub>4</sub> -Based Photocatalysts for Hydrogen Generation. Journal of Physical Chemistry Letters, 2014, 5, 2101-2107.	4.6	1,107
21	Hydrogen Production by Photocatalytic Water Splitting over Pt/TiO <sub>2</sub> Nanosheets with Exposed (001) Facets. Journal of Physical Chemistry C, 2010, 114, 13118-13125.	3.1	1,071
22	Hierarchical Porous Oâ€Doped g <sub>3</sub> N <sub>4</sub> with Enhanced Photocatalytic CO <sub>2</sub> Reduction Activity. Small, 2017, 13, 1603938.	10.0	1,025
23	New understanding of the difference of photocatalytic activity among anatase, rutile and brookite TiO <sub>2</sub> . Physical Chemistry Chemical Physics, 2014, 16, 20382-20386.	2.8	990
24	Surface modification and enhanced photocatalytic CO2 reduction performance of TiO2: a review. Applied Surface Science, 2017, 392, 658-686.	6.1	989
25	Tunable Photocatalytic Selectivity of Hollow TiO <sub>2</sub> Microspheres Composed of Anatase Polyhedra with Exposed {001} Facets. Journal of the American Chemical Society, 2010, 132, 11914-11916.	13.7	979
26	A Review of Direct Zâ $\in$ Scheme Photocatalysts. Small Methods, 2017, 1, 1700080.	8.6	955
27	Sulfur-doped g-C3N4 with enhanced photocatalytic CO2-reduction performance. Applied Catalysis B: Environmental, 2015, 176-177, 44-52.	20.2	919
28	Review on the improvement of the photocatalytic and antibacterial activities of ZnO. Journal of Alloys and Compounds, 2017, 727, 792-820.	5.5	884
29	Visible Light Photocatalytic H <sub>2</sub> -Production Activity of CuS/ZnS Porous Nanosheets Based on Photoinduced Interfacial Charge Transfer. Nano Letters, 2011, 11, 4774-4779.	9.1	846
30	Noble Metal-Free Reduced Graphene Oxide-Zn <sub><i>x</i></sub> Cd <sub>1–<i>x</i></sub> S Nanocomposite with Enhanced Solar Photocatalytic H <sub>2</sub> -Production Performance. Nano Letters, 2012, 12, 4584-4589.	9.1	845
31	Graphene in Photocatalysis: A Review. Small, 2016, 12, 6640-6696.	10.0	836
32	Designing a 0D/2D Sâ€Scheme Heterojunction over Polymeric Carbon Nitride for Visibleâ€Light Photocatalytic Inactivation of Bacteria. Angewandte Chemie - International Edition, 2020, 59, 5218-5225.	13.8	822
33	An overview on the removal of synthetic dyes from water by electrochemical advanced oxidation processes. Chemosphere, 2018, 197, 210-227.	8.2	814
34	Dual Cocatalysts in TiO <sub>2</sub> Photocatalysis. Advanced Materials, 2019, 31, e1807660.	21.0	796
35	Unique S-scheme heterojunctions in self-assembled TiO2/CsPbBr3 hybrids for CO2 photoreduction. Nature Communications, 2020, 11, 4613.	12.8	776
36	Fabrication and Characterization of Visible-Light-Driven Plasmonic Photocatalyst Ag/AgCl/TiO <sub>2</sub> Nanotube Arrays. Journal of Physical Chemistry C, 2009, 113, 16394-16401.	3.1	770

#	Article	IF	CITATIONS
37	Efficient Visible-Light-Induced Photocatalytic Disinfection on Sulfur-Doped Nanocrystalline Titania. Environmental Science & Technology, 2005, 39, 1175-1179.	10.0	754
38	Hydrothermal Synthesis and Photocatalytic Activity of Zinc Oxide Hollow Spheres. Environmental Science & Technology, 2008, 42, 4902-4907.	10.0	754
39	Isoelectric point and adsorption activity of porous g-C3N4. Applied Surface Science, 2015, 344, 188-195.	6.1	753
40	Efficient Visible-Light Photocatalytic Hydrogen Evolution and Enhanced Photostability of Core/Shell CdS/g-C <sub>3</sub> N <sub>4</sub> Nanowires. ACS Applied Materials & Interfaces, 2013, 5, 10317-10324.	8.0	747
41	Enhanced photocatalytic H2-production activity of graphene-modified titania nanosheets. Nanoscale, 2011, 3, 3670.	5.6	742
42	A direct Z-scheme g-C3N4/SnS2 photocatalyst with superior visible-light CO2 reduction performance. Journal of Catalysis, 2017, 352, 532-541.	6.2	721
43	Product selectivity of photocatalytic CO2 reduction reactions. Materials Today, 2020, 32, 222-243.	14.2	719
44	Emerging Sâ€Scheme Photocatalyst. Advanced Materials, 2022, 34, e2107668.	21.0	717
45	In Situ Irradiated Xâ€Ray Photoelectron Spectroscopy Investigation on a Direct Zâ€Scheme TiO <sub>2</sub> /CdS Composite Film Photocatalyst. Advanced Materials, 2019, 31, e1802981.	21.0	714
46	Metalâ€Free 2D/2D Phosphorene/g <sub>3</sub> N <sub>4</sub> Van der Waals Heterojunction for Highly Enhanced Visibleâ€Light Photocatalytic H <sub>2</sub> Production. Advanced Materials, 2018, 30, e1800128.	21.0	707
47	Preparation, characterization and visible-light-driven photocatalytic activity of Fe-doped titania nanorods and first-principles study for electronic structures. Applied Catalysis B: Environmental, 2009, 90, 595-602.	20.2	700
48	CdS/Graphene Nanocomposite Photocatalysts. Advanced Energy Materials, 2015, 5, 1500010.	19.5	694
49	Grapheneâ€Based Photocatalysts for Solarâ€Fuel Generation. Angewandte Chemie - International Edition, 2015, 54, 11350-11366.	13.8	692
50	A Hierarchical Z-Scheme CdS-WO <sub>3</sub> Photocatalyst with Enhanced CO <sub>2</sub> Reduction Activity. Small, 2015, 11, 5262-5271.	10.0	682
51	Anatase TiO <sub>2</sub> with Dominant High-Energy {001} Facets: Synthesis, Properties, and Applications. Chemistry of Materials, 2011, 23, 4085-4093.	6.7	669
52	Fabrication and characterization of Ag–TiO2 multiphase nanocomposite thin films with enhanced photocatalytic activity. Applied Catalysis B: Environmental, 2005, 60, 211-221.	20.2	660
53	Direct Z-scheme ZnO/CdS hierarchical photocatalyst for enhanced photocatalytic H2-production activity. Applied Catalysis B: Environmental, 2019, 243, 19-26.	20.2	653
54	TiO2/MXene Ti3C2 composite with excellent photocatalytic CO2 reduction activity. Journal of Catalysis, 2018, 361, 255-266.	6.2	647

#	Article	IF	CITATIONS
55	Templateâ€Free Fabrication and Enhanced Photocatalytic Activity of Hierarchical Macroâ€∕Mesoporous Titania. Advanced Functional Materials, 2007, 17, 1984-1990.	14.9	635
56	Ultra-thin nanosheet assemblies of graphitic carbon nitride for enhanced photocatalytic CO <sub>2</sub> reduction. Journal of Materials Chemistry A, 2017, 5, 3230-3238.	10.3	621
57	2D/2D/0D TiO2/C3N4/Ti3C2 MXene composite S-scheme photocatalyst with enhanced CO2 reduction activity. Applied Catalysis B: Environmental, 2020, 272, 119006.	20.2	604
58	Fabrication and photocatalytic activity enhanced mechanism of direct Z-scheme g-C 3 N 4 /Ag 2 WO 4 photocatalyst. Applied Surface Science, 2017, 391, 175-183.	6.1	601
59	Use of surfactants for the remediation of contaminated soils: A review. Journal of Hazardous Materials, 2015, 285, 419-435.	12.4	597
60	Quantitative characterization of hydroxyl radicals produced by various photocatalysts. Journal of Colloid and Interface Science, 2011, 357, 163-167.	9.4	592
61	Enhancement of Photocatalytic Activity of Mesporous TiO <sub>2</sub> Powders by Hydrothermal Surface Fluorination Treatment. Journal of Physical Chemistry C, 2009, 113, 6743-6750.	3.1	577
62	Size- and shape-dependent catalytic performances of oxidation and reduction reactions on nanocatalysts. Chemical Society Reviews, 2016, 45, 4747-4765.	38.1	568
63	Zn <sub>1–<i>x</i></sub> Cd <sub><i>x</i></sub> S Solid Solutions with Controlled Bandgap and Enhanced Visible-Light Photocatalytic H <sub>2</sub> -Production Activity. ACS Catalysis, 2013, 3, 882-889.	11.2	565
64	Facile preparation and enhanced photocatalytic H2-production activity of Cu(OH)2 cluster modified TiO2. Energy and Environmental Science, 2011, 4, 1364.	30.8	554
65	Two-dimensional layered composite photocatalysts. Chemical Communications, 2014, 50, 10768.	4.1	551
66	An Inorganic/Organic Sâ€5cheme Heterojunction H <sub>2</sub> â€Production Photocatalyst and its Charge Transfer Mechanism. Advanced Materials, 2021, 33, e2100317.	21.0	528
67	Effect of surface structure on photocatalytic activity of TiO2 thin films prepared by sol-gel method. Thin Solid Films, 2000, 379, 7-14.	1.8	519
68	Preparation and Photocatalytic Behavior of MoS2 and WS2 Nanocluster Sensitized TiO2. Langmuir, 2004, 20, 5865-5869.	3.5	519
69	2D/2D g-C <sub>3</sub> N <sub>4</sub> /MnO <sub>2</sub> Nanocomposite as a Direct Z-Scheme Photocatalyst for Enhanced Photocatalytic Activity. ACS Sustainable Chemistry and Engineering, 2018, 6, 965-973.	6.7	519
70	Effects of acidic and basic hydrolysis catalysts on the photocatalytic activity and microstructures of bimodal mesoporous titania. Journal of Catalysis, 2003, 217, 69-69.	6.2	518
71	In Situ Grown Monolayer Nâ€Doped Graphene on CdS Hollow Spheres with Seamless Contact for Photocatalytic CO <sub>2</sub> Reduction. Advanced Materials, 2019, 31, e1902868.	21.0	515
72	A review on TiO2-based Z-scheme photocatalysts. Chinese Journal of Catalysis, 2017, 38, 1936-1955.	14.0	511

#	Article	IF	CITATIONS
73	Pivotal role of fluorine in enhanced photocatalytic activity of anatase TiO2 nanosheets with dominant (001) facets for the photocatalytic degradation of acetone in air. Applied Catalysis B: Environmental, 2010, 96, 557-564.	20.2	509
74	Synthesis and Enhanced Visible-Light Photoelectrocatalytic Activity of <i>p</i> â^' <i>n</i> Junction BiOI/TiO <sub>2</sub> Nanotube Arrays. Journal of Physical Chemistry C, 2011, 115, 7339-7346.	3.1	503
75	Graphene-Based Photocatalysts for Hydrogen Generation. Journal of Physical Chemistry Letters, 2013, 4, 753-759.	4.6	501
76	A noble metal-free reduced graphene oxide–CdS nanorod composite for the enhanced visible-light photocatalytic reduction of CO2 to solar fuel. Journal of Materials Chemistry A, 2014, 2, 3407.	10.3	499
77	Sulfur-doped g-C3N4/TiO2 S-scheme heterojunction photocatalyst for Congo Red photodegradation. Chinese Journal of Catalysis, 2021, 42, 56-68.	14.0	493
78	Enhanced photocatalytic activity and stability of Z-scheme Ag2CrO4-GO composite photocatalysts for organic pollutant degradation. Applied Catalysis B: Environmental, 2015, 164, 380-388.	20.2	483
79	Recent advances in visible light Bi-based photocatalysts. Chinese Journal of Catalysis, 2014, 35, 989-1007.	14.0	481
80	Enhanced photocatalytic activity of mesoporous TiO <sub>2</sub> aggregates by embedding carbon nanotubes as electron-transfer channel. Physical Chemistry Chemical Physics, 2011, 13, 3491-3501.	2.8	476
81	Ag2CrO4/g-C3N4/graphene oxide ternary nanocomposite Z-scheme photocatalyst with enhanced CO2 reduction activity. Applied Catalysis B: Environmental, 2018, 231, 368-380.	20.2	469
82	Photocatalytic reduction of CO2 into hydrocarbon solar fuels over g-C3N4–Pt nanocomposite photocatalysts. Physical Chemistry Chemical Physics, 2014, 16, 11492.	2.8	465
83	Surface plasmon resonance-mediated photocatalysis by noble metal-based composites under visible light. Journal of Materials Chemistry, 2012, 22, 21337.	6.7	462
84	A new understanding of the photocatalytic mechanism of the direct Z-scheme g-C <sub>3</sub> N <sub>4</sub> /TiO <sub>2</sub> heterostructure. Physical Chemistry Chemical Physics, 2016, 18, 31175-31183.	2.8	459
85	Enhanced photocatalytic H2-production activity of WO3/TiO2 step-scheme heterojunction by graphene modification. Chinese Journal of Catalysis, 2020, 41, 9-20.	14.0	458
86	Enhanced photocatalytic activity of mesoporous and ordinary TiO2 thin films by sulfuric acid treatment. Applied Catalysis B: Environmental, 2002, 36, 31-43.	20.2	450
87	Template-free Hydrothermal Synthesis of CuO/Cu <sub>2</sub> O Composite Hollow Microspheres. Chemistry of Materials, 2007, 19, 4327-4334.	6.7	450
88	In situ Irradiated XPS Investigation on Sâ€5cheme TiO <sub>2</sub> @ZnIn <sub>2</sub> S <sub>4</sub> Photocatalyst for Efficient Photocatalytic CO <sub>2</sub> Reduction. Small, 2021, 17, e2103447.	10.0	449
89	Design and fabrication of semiconductor photocatalyst for photocatalytic reduction of CO2 to solar fuel. Science China Materials, 2014, 57, 70-100.	6.3	446
90	Hydrothermal Preparation and Photocatalytic Activity of Hierarchically Sponge-like Macro-/Mesoporous Titania. Journal of Physical Chemistry C, 2007, 111, 10582-10589.	3.1	443

#	Article	IF	CITATIONS
91	Review on Metal Sulphideâ€based Zâ€scheme Photocatalysts. ChemCatChem, 2019, 11, 1394-1411.	3.7	439
92	Enhancement of photocatalytic activity of mesoporous TiO2 by using carbon nanotubes. Applied Catalysis A: General, 2005, 289, 186-196.	4.3	434
93	Anatase TiO2 nanosheets with exposed (001) facets: improved photoelectric conversion efficiency in dye-sensitized solar cells. Nanoscale, 2010, 2, 2144.	5.6	423
94	Ag <sub>2</sub> O as a New Visibleâ€Light Photocatalyst: Selfâ€Stability and High Photocatalytic Activity. Chemistry - A European Journal, 2011, 17, 7777-7780.	3.3	423
95	First principle investigation of halogen-doped monolayer g-C3N4 photocatalyst. Applied Catalysis B: Environmental, 2017, 207, 27-34.	20.2	422
96	Review on nanoscale Bi-based photocatalysts. Nanoscale Horizons, 2018, 3, 464-504.	8.0	421
97	Superb adsorption capacity of hierarchical calcined Ni/Mg/Al layered double hydroxides for Congo red and Cr(VI) ions. Journal of Hazardous Materials, 2017, 321, 801-811.	12.4	417
98	Noble metal-free Ni(OH)2–g-C3N4 composite photocatalyst with enhanced visible-light photocatalytic H2-production activity. Catalysis Science and Technology, 2013, 3, 1782.	4.1	411
99	Fabrication of Hollow Inorganic Microspheres by Chemically Induced Self-Transformation. Advanced Functional Materials, 2006, 16, 2035-2041.	14.9	407
100	CulnS2 sensitized TiO2 hybrid nanofibers for improved photocatalytic CO2 reduction. Applied Catalysis B: Environmental, 2018, 230, 194-202.	20.2	407
101	Constructing 2D/2D Fe <sub>2</sub> O <sub>3</sub> /g <sub>3</sub> N <sub>4</sub> Direct Z cheme Photocatalysts with Enhanced H <sub>2</sub> Generation Performance. Solar Rrl, 2018, 2, 1800006.	5.8	403
102	Effects of Fe-doping on the photocatalytic activity of mesoporous TiO2 powders prepared by an ultrasonic method. Journal of Hazardous Materials, 2006, 137, 1838-1847.	12.4	401
103	One-step synthesis of easy-recycling TiO2-rGO nanocomposite photocatalysts with enhanced photocatalytic activity. Applied Catalysis B: Environmental, 2013, 132-133, 452-459.	20.2	396
104	Novel urea assisted hydrothermal synthesis of hierarchical BiVO4/Bi2O2CO3 nanocomposites with enhanced visible-light photocatalytic activity. Applied Catalysis B: Environmental, 2011, 110, 286-295.	20.2	392
105	Enhanced Photocatalytic H <sub>2</sub> -Production Activity of TiO <sub>2</sub> by Ni(OH) <sub>2</sub> Cluster Modification. Journal of Physical Chemistry C, 2011, 115, 4953-4958.	3.1	392
106	Fabrication and enhanced visible-light photocatalytic activity of carbon self-doped TiO <sub>2</sub> sheets with exposed {001} facets. Journal of Materials Chemistry, 2011, 21, 1049-1057.	6.7	390
107	Effect of calcination temperature on morphology and photoelectrochemical properties of anodized titanium dioxide nanotube arrays. Applied Catalysis B: Environmental, 2010, 94, 295-302.	20.2	388
108	First-principle calculation study of tri-s-triazine-based g-C3N4: A review. Applied Catalysis B: Environmental, 2018, 224, 983-999.	20.2	382

#	Article	IF	CITATIONS
109	Semiconductor-based photocatalytic CO <sub>2</sub> conversion. Materials Horizons, 2015, 2, 261-278.	12.2	380
110	Enhanced photocatalytic H 2 -production activity of anatase TiO 2 nanosheet by selectively depositing dual-cocatalysts on {101} and {001} facets. Applied Catalysis B: Environmental, 2016, 198, 286-294.	20.2	375
111	Graphene-Based Photocatalysts for CO <sub>2</sub> Reduction to Solar Fuel. Journal of Physical Chemistry Letters, 2015, 6, 4244-4251.	4.6	368
112	Direct Observation of Structural Evolution of Metal Chalcogenide in Electrocatalytic Water Oxidation. ACS Nano, 2018, 12, 12369-12379.	14.6	366
113	Self-assembled hierarchical direct Z-scheme g-C3N4/ZnO microspheres with enhanced photocatalytic CO2 reduction performance. Applied Surface Science, 2018, 441, 12-22.	6.1	364
114	Ni(OH)2 modified CdS nanorods for highly efficient visible-light-driven photocatalytic H2 generation. Green Chemistry, 2011, 13, 2708.	9.0	363
115	The effect of manganese vacancy in birnessite-type MnO2 on room-temperature oxidation of formaldehyde in air. Applied Catalysis B: Environmental, 2017, 204, 147-155.	20.2	362
116	Microstructures and photoactivity of mesoporous anatase hollow microspheres fabricated by fluoride-mediated self-transformation. Journal of Catalysis, 2007, 249, 59-66.	6.2	359
117	Morphology-dependent photocatalytic H2-production activity of CdS. Applied Catalysis B: Environmental, 2014, 156-157, 184-191.	20.2	359
118	Enhanced photocatalytic activity of hierarchical macro/mesoporous TiO2–graphene composites for photodegradation of acetone in air. Applied Catalysis B: Environmental, 2012, 119-120, 109-116.	20.2	356
119	Making co-condensed amorphous carbon/g-C3N4 composites with improved visible-light photocatalytic H2-production performance using Pt as cocatalyst. Carbon, 2017, 118, 241-249.	10.3	356
120	Enhanced Performance of NaOH-Modified Pt/TiO <sub>2</sub> toward Room Temperature Selective Oxidation of Formaldehyde. Environmental Science & Technology, 2013, 47, 2777-2783.	10.0	355
121	A critical review of the application of chelating agents to enable Fenton and Fenton-like reactions at high pH values. Journal of Hazardous Materials, 2019, 362, 436-450.	12.4	353
122	Effects of calcination temperature on the microstructures and photocatalytic activity of titanate nanotubes. Journal of Molecular Catalysis A, 2006, 249, 135-142.	4.8	352
123	Synthesis of hierarchical Ni(OH)2 and NiO nanosheets and their adsorption kinetics and isotherms to Congo red in water. Journal of Hazardous Materials, 2011, 185, 889-897.	12.4	343
124	Hollow CoS <sub><i>x</i></sub> Polyhedrons Act as High-Efficiency Cocatalyst for Enhancing the Photocatalytic Hydrogen Generation of g-C <sub>3</sub> N <sub>4</sub> . ACS Sustainable Chemistry and Engineering, 2018, 6, 2767-2779.	6.7	343
125	Nitrogen self-doped nanosized TiO2 sheets with exposed {001} facets for enhanced visible-light photocatalytic activity. Chemical Communications, 2011, 47, 6906.	4.1	342
126	Facet effect of Pd cocatalyst on photocatalytic CO 2 reduction over g-C 3 N 4. Journal of Catalysis, 2017, 349, 208-217.	6.2	332

#	Article	IF	CITATIONS
127	Photocatalytic activity of nanometer TiO2 thin films prepared by the sol–gel method. Materials Chemistry and Physics, 2001, 69, 25-29.	4.0	329
128	3D hierarchical graphene oxide-NiFe LDH composite with enhanced adsorption affinity to Congo red, methyl orange and Cr(VI) ions. Journal of Hazardous Materials, 2019, 369, 214-225.	12.4	329
129	Challenges for photocatalytic overall water splitting. CheM, 2022, 8, 1567-1574.	11.7	329
130	Improved visible-light photocatalytic activity of porous carbon self-doped ZnO nanosheet-assembled flowers. CrystEngComm, 2011, 13, 2533.	2.6	328
131	Enhanced visible light photocatalytic H2-production of g-C3N4/WS2 composite heterostructures. Applied Surface Science, 2015, 358, 196-203.	6.1	327
132	TiO2 nanosheets with exposed {001} facets for photocatalytic applications. Nano Research, 2016, 9, 3-27.	10.4	327
133	Direct Sonochemical Preparation and Characterization of Highly Active Mesoporous TiO2 with a Bicrystalline Framework. Chemistry of Materials, 2002, 14, 4647-4653.	6.7	325
134	Tailoring the energy band gap and edges' potentials of g-C 3 N 4 /TiO 2 composite photocatalysts for NO x removal. Chemical Engineering Journal, 2017, 310, 571-580.	12.7	325
135	Highly efficient electrosynthesis of hydrogen peroxide on a superhydrophobic three-phase interface by natural air diffusion. Nature Communications, 2020, 11, 1731.	12.8	325
136	Design, Fabrication, and Mechanism of Nitrogenâ€Đoped Grapheneâ€Based Photocatalyst. Advanced Materials, 2021, 33, e2003521.	21.0	324
137	Fabrication of NiS modified CdS nanorod p–n junction photocatalysts with enhanced visible-light photocatalytic H2-production activity. Physical Chemistry Chemical Physics, 2013, 15, 12088.	2.8	323
138	Preparation of highly photocatalytic active nano-sized TiO2 particles via ultrasonic irradiation. Chemical Communications, 2001, , 1942-1943.	4.1	321
139	Preparation and enhanced visible-light photocatalytic H2-production activity of CdS quantum dots-sensitized Zn1â"xCdxS solid solution. Green Chemistry, 2010, 12, 1611.	9.0	321
140	Microwave-assisted hydrothermal synthesis of graphene based Au–TiO <sub>2</sub> photocatalysts for efficient visible-light hydrogen production. Journal of Materials Chemistry A, 2014, 2, 3847-3855.	10.3	314
141	Pt Single Atoms Supported on Nâ€Doped Mesoporous Hollow Carbon Spheres with Enhanced Electrocatalytic H <sub>2</sub> â€Evolution Activity. Advanced Materials, 2021, 33, e2008599.	21.0	314
142	Core–Shell Nitrogenâ€Đoped Carbon Hollow Spheres/Co <sub>3</sub> O <sub>4</sub> Nanosheets as Advanced Electrode for Highâ€Performance Supercapacitor. Small, 2018, 14, e1702407.	10.0	309
143	Metal–Organic Framework-Derived Nickel–Cobalt Sulfide on Ultrathin Mxene Nanosheets for Electrocatalytic Oxygen Evolution. ACS Applied Materials & Interfaces, 2018, 10, 22311-22319.	8.0	306
144	TiO2/polydopamine S-scheme heterojunction photocatalyst with enhanced CO2-reduction selectivity. Applied Catalysis B: Environmental, 2021, 289, 120039.	20.2	302

#	Article	IF	CITATIONS
145	Recent advances in g-C3N4-based heterojunction photocatalysts. Journal of Materials Science and Technology, 2020, 56, 1-17.	10.7	297
146	Photocatalytic hydrogen production over CuO-modified titania. Journal of Colloid and Interface Science, 2011, 357, 223-228.	9.4	292
147	Hydrothermal Synthesis and Visible-light Photocatalytic Activity of Novel Cage-like Ferric Oxide Hollow Spheres. Crystal Growth and Design, 2009, 9, 1474-1480.	3.0	291
148	Hydrothermal preparation and visible-light photocatalytic activity of Bi2WO6 powders. Journal of Solid State Chemistry, 2005, 178, 1968-1972.	2.9	288
149	The synergistic effect of graphitic N and pyrrolic N for the enhanced photocatalytic performance of nitrogen-doped graphene/TiO2 nanocomposites. Applied Catalysis B: Environmental, 2016, 181, 810-817.	20.2	287
150	In Situ Fabrication of Ni–Mo Bimetal Sulfide Hybrid as an Efficient Electrocatalyst for Hydrogen Evolution over a Wide pH Range. ACS Catalysis, 2017, 7, 6179-6187.	11.2	287
151	Singleâ€Atom Engineering of Directional Charge Transfer Channels and Active Sites for Photocatalytic Hydrogen Evolution. Advanced Functional Materials, 2018, 28, 1802169.	14.9	287
152	Sâ€ <b>s</b> cheme Heterojunction TiO <sub>2</sub> /CdS Nanocomposite Nanofiber as H <sub>2</sub> â€Production Photocatalyst. ChemCatChem, 2019, 11, 6301-6309.	3.7	286
153	Photocatalytic H2 evolution on graphdiyne/g-C3N4 hybrid nanocomposites. Applied Catalysis B: Environmental, 2019, 255, 117770.	20.2	284
154	Nitrogen and sulfur co-doped TiO <sub>2</sub> nanosheets with exposed {001} facets: synthesis, characterization and visible-light photocatalytic activity. Physical Chemistry Chemical Physics, 2011, 13, 4853-4861.	2.8	282
155	Simultaneously Tuning Charge Separation and Oxygen Reduction Pathway on Graphitic Carbon Nitride by Polyethylenimine for Boosted Photocatalytic Hydrogen Peroxide Production. ACS Catalysis, 2020, 10, 3697-3706.	11.2	275
156	Ion-Exchange Synthesis and Enhanced Visible-Light Photoactivity of CuS/ZnS Nanocomposite Hollow Spheres. Journal of Physical Chemistry C, 2010, 114, 13642-13649.	3.1	274
157	Effect of Crystallization Methods on Morphology and Photocatalytic Activity of Anodized TiO <sub>2</sub> Nanotube Array Films. Journal of Physical Chemistry C, 2010, 114, 19378-19385.	3.1	271
158	MXene-based photocatalysts. Journal of Materials Science and Technology, 2020, 56, 18-44.	10.7	269
159	S-scheme heterojunction based on p-type ZnMn2O4 and n-type ZnO with improved photocatalytic CO2 reduction activity. Chemical Engineering Journal, 2021, 409, 127377.	12.7	269
160	Facile Synthesis of Ordered Mesoporous Alumina and Alumina-Supported Metal Oxides with Tailored Adsorption and Framework Properties. Chemistry of Materials, 2011, 23, 1147-1157.	6.7	268
161	Non-Noble Plasmonic Metal-Based Photocatalysts. Chemical Reviews, 2022, 122, 10484-10537.	47.7	268
162	Synthesis of hierarchical porous zinc oxide (ZnO) microspheres with highly efficient adsorption of Congo red. Journal of Colloid and Interface Science, 2017, 490, 242-251.	9.4	266

#	Article	IF	CITATIONS
163	Enhanced visible-light photocatalytic activity of Bi2WO6 nanoparticles by Ag2O cocatalyst. Applied Catalysis B: Environmental, 2012, 111-112, 326-333.	20.2	259
164	Facetâ€Mediated Photodegradation of Organic Dye over Hematite Architectures by Visible Light. Angewandte Chemie - International Edition, 2012, 51, 178-182.	13.8	258
165	Unraveling Photoexcited Charge Transfer Pathway and Process of CdS/Graphene Nanoribbon Composites toward Visibleâ€Light Photocatalytic Hydrogen Evolution. Small, 2019, 15, e1902459.	10.0	258
166	Enhanced visible-light photocatalytic activity of plasmonic Ag and graphene co-modified Bi <sub>2</sub> WO <sub>6</sub> nanosheets. Physical Chemistry Chemical Physics, 2014, 16, 1111-1120.	2.8	256
167	H <sub>2</sub> WO <sub>4</sub> ·H <sub>2</sub> O/Ag/AgCl Composite Nanoplates: A Plasmonic Z-Scheme Visible-Light Photocatalyst. Journal of Physical Chemistry C, 2011, 115, 14648-14655.	3.1	255
168	Enhanced photocatalytic activity of TiO2 powder (P25) by hydrothermal treatment. Journal of Molecular Catalysis A, 2006, 253, 112-118.	4.8	254
169	Heterogeneous electro-Fenton using modified iron–carbon as catalyst for 2,4-dichlorophenol degradation: Influence factors, mechanism and degradation pathway. Water Research, 2015, 70, 414-424.	11.3	254
170	Designing Defective Crystalline Carbon Nitride to Enable Selective CO <sub>2</sub> Photoreduction in the Gas Phase. Advanced Functional Materials, 2019, 29, 1900093.	14.9	254
171	A New Approach for Photocorrosion Inhibition of Ag <sub>2</sub> CO <sub>3</sub> Photocatalyst with Highly Visible-Light-Responsive Reactivity. Journal of Physical Chemistry C, 2012, 116, 15519-15524.	3.1	253
172	Carbon-based H2-production photocatalytic materials. Journal of Photochemistry and Photobiology C: Photochemistry Reviews, 2016, 27, 72-99.	11.6	252
173	Tunable photocatalytic selectivity of TiO2 films consisted of flower-like microspheres with exposed {001} facets. Chemical Communications, 2011, 47, 4532.	4.1	250
174	Hierarchical porous CdS nanosheet-assembled flowers with enhanced visible-light photocatalytic H2-production performance. Applied Catalysis B: Environmental, 2013, 138-139, 299-303.	20.2	249
175	Step-scheme CdS/TiO2 nanocomposite hollow microsphere with enhanced photocatalytic CO2 reduction activity. Journal of Materials Science and Technology, 2020, 56, 143-150.	10.7	249
176	Effects of calcination temperature on the photocatalytic activity and photo-induced super-hydrophilicity of mesoporous TiO2 thin films. New Journal of Chemistry, 2002, 26, 607-613.	2.8	247
177	Microbial fuel cell (MFC) power performance improvement through enhanced microbial electrogenicity. Biotechnology Advances, 2018, 36, 1316-1327.	11.7	247
178	Nickel-based materials for supercapacitors. Materials Today, 2019, 25, 35-65.	14.2	247
179	Dye-sensitized solar cells based on anatase TiO2 hollow spheres/carbon nanotube composite films. Journal of Power Sources, 2011, 196, 7891-7898.	7.8	245
180	A One-Pot Approach to Hierarchically Nanoporous Titania Hollow Microspheres with High Photocatalytic Activity. Crystal Growth and Design, 2008, 8, 930-934.	3.0	244

#	Article	IF	CITATIONS
181	Ternary NiS/Zn <i><sub>x</sub></i> Cd <sub>1â€<i>x</i></sub> S/Reduced Graphene Oxide Nanocomposites for Enhanced Solar Photocatalytic H <sub>2</sub> â€Production Activity. Advanced Energy Materials, 2014, 4, 1301925.	19.5	244
182	0D/3D MoS2-NiS2/N-doped graphene foam composite for efficient overall water splitting. Applied Catalysis B: Environmental, 2019, 254, 15-25.	20.2	243
183	One-step hydrothermal fabrication and photocatalytic activity of surface-fluorinated TiO <sub>2</sub> hollow microspheres and tabular anatase single micro-crystals with high-energy facets. CrystEngComm, 2010, 12, 872-879.	2.6	241
184	g-C3N4 modified TiO2 nanosheets with enhanced photoelectric conversion efficiency in dye-sensitized solar cells. Journal of Power Sources, 2015, 274, 77-84.	7.8	241
185	Hybrid carbon@TiO <sub>2</sub> hollow spheres with enhanced photocatalytic CO <sub>2</sub> reduction activity. Journal of Materials Chemistry A, 2017, 5, 5020-5029.	10.3	240
186	Preparation and enhanced visible-light photocatalytic H2-production activity of CdS-sensitized Pt/TiO2 nanosheets with exposed (001) facets. Physical Chemistry Chemical Physics, 2011, 13, 8915.	2.8	235
187	UV- and Visible-Light Photocatalytic Activity of Simultaneously Deposited and Doped Ag/Ag(I)-TiO <sub>2</sub> Photocatalyst. Journal of Physical Chemistry C, 2012, 116, 17721-17728.	3.1	233
188	Highly dispersed TiO2 nanocrystals and WO3 nanorods on reduced graphene oxide: Z-scheme photocatalysis system for accelerated photocatalytic water disinfection. Applied Catalysis B: Environmental, 2017, 218, 163-173.	20.2	233
189	Graphdiyne-modified TiO2 nanofibers with osteoinductive and enhanced photocatalytic antibacterial activities to prevent implant infection. Nature Communications, 2020, 11, 4465.	12.8	233
190	Preparation and enhanced photocatalytic activity of Ag@TiO2 core–shell nanocomposite nanowires. Journal of Hazardous Materials, 2010, 177, 971-977.	12.4	232
191	Template-free synthesis of hierarchical spindle-like γ-Al2O3 materials and their adsorption affinity towards organic and inorganic pollutants in water. Journal of Materials Chemistry, 2010, 20, 4587.	6.7	232
192	Oneâ€Pot Templateâ€Free Synthesis of Monodisperse Zinc Sulfide Hollow Spheres and Their Photocatalytic Properties. Chemistry - A European Journal, 2009, 15, 6731-6739.	3.3	229
193	Efficient photocatalytic reduction of CO2 by amine-functionalized g-C3N4. Applied Surface Science, 2015, 358, 350-355.	6.1	229
194	High-efficiency degradation of organic pollutants with Fe, N co-doped biochar catalysts via persulfate activation. Journal of Hazardous Materials, 2020, 397, 122764.	12.4	224
195	Amorphous molybdenum sulfide as highly efficient electron-cocatalyst for enhanced photocatalytic H2 evolution. Applied Catalysis B: Environmental, 2016, 193, 217-225.	20.2	223
196	Enhanced Photocatalytic Hydrogen Production Activities of Au-Loaded ZnS Flowers. ACS Applied Materials & Interfaces, 2013, 5, 1031-1037.	8.0	221
197	Hollow Carbon Spheres and Their Hybrid Nanomaterials in Electrochemical Energy Storage. Advanced Energy Materials, 2019, 9, 1803900.	19.5	220
198	Structure effect of graphene on the photocatalytic performance of plasmonic Ag/Ag2CO3-rGO for photocatalytic elimination of pollutants. Applied Catalysis B: Environmental, 2016, 181, 71-78.	20.2	219

#	Article	IF	CITATIONS
199	TiO <sub>2</sub> –MnO <sub><i>x</i></sub> –Pt Hybrid Multiheterojunction Film Photocatalyst with Enhanced Photocatalytic CO <sub>2</sub> -Reduction Activity. ACS Applied Materials & Interfaces, 2019, 11, 5581-5589.	8.0	219
200	Hollow Iron–Vanadium Composite Spheres: A Highly Efficient Ironâ€Based Water Oxidation Electrocatalyst without the Need for Nickel or Cobalt. Angewandte Chemie - International Edition, 2017, 56, 3289-3293.	13.8	216
201	Direct Z-Scheme TiO <sub>2</sub> /NiS Core–Shell Hybrid Nanofibers with Enhanced Photocatalytic H <sub>2</sub> -Production Activity. ACS Sustainable Chemistry and Engineering, 2018, 6, 12291-12298.	6.7	216
202	Direct Z-scheme anatase/rutile bi-phase nanocomposite TiO 2 nanofiber photocatalyst with enhanced photocatalytic H 2 -production activity. International Journal of Hydrogen Energy, 2014, 39, 15394-15402.	7.1	213
203	Enhanced photocatalytic H2 production on CdS nanorod using cobalt-phosphate as oxidation cocatalyst. Applied Surface Science, 2016, 389, 775-782.	6.1	212
204	New understanding on the different photocatalytic activity of wurtzite and zinc-blende CdS. Applied Catalysis B: Environmental, 2016, 192, 101-107.	20.2	212
205	Hierarchical TiO <sub>2</sub> /Ni(OH) <sub>2</sub> composite fibers with enhanced photocatalytic CO <sub>2</sub> reduction performance. Journal of Materials Chemistry A, 2018, 6, 4729-4736.	10.3	212
206	Effect of calcination temperature on morphology and photocatalytic activity of anatase TiO2 nanosheets with exposed {0 0 1} facets. Applied Catalysis B: Environmental, 2011, 104, 275-281.	20.2	211
207	Recent advances in microbial fuel cells ( <scp>MFCs</scp> ) and microbial electrolysis cells ( <scp>MECs</scp> ) for wastewater treatment, bioenergy and bioproducts. Journal of Chemical Technology and Biotechnology, 2013, 88, 508-518.	3.2	211
208	Preparation, characterization and photocatalytic activity of in situ N,S-codoped TiO2 powders. Journal of Molecular Catalysis A, 2006, 246, 176-184.	4.8	210
209	Superparamagnetic γ-Fe2O3@SiO2@TiO2 composite microspheres with superior photocatalytic properties. Applied Catalysis B: Environmental, 2011, 104, 12-20.	20.2	209
210	Cubic anatase TiO <sub>2</sub> nanocrystals with enhanced photocatalytic CO <sub>2</sub> reduction activity. Chemical Communications, 2015, 51, 7950-7953.	4.1	209
211	A simple template-free approach to TiO2 hollow spheres with enhanced photocatalytic activity. Dalton Transactions, 2010, 39, 5860.	3.3	208
212	Oxygen vacancies in metal oxides: recent progress towards advanced catalyst design. Science China Materials, 2020, 63, 2089-2118.	6.3	208
213	Graphdiyne: A New Photocatalytic CO <sub>2</sub> Reduction Cocatalyst. Advanced Functional Materials, 2019, 29, 1904256.	14.9	207
214	Curved Surface Boosts Electrochemical CO <sub>2</sub> Reduction to Formate via Bismuth Nanotubes in a Wide Potential Window. ACS Catalysis, 2020, 10, 358-364.	11.2	206
215	Trace-level phosphorus and sodium co-doping of g-C 3 N 4 for enhanced photocatalytic H 2 production. Journal of Power Sources, 2017, 351, 151-159.	7.8	205
216	A simple cation exchange approach to Bi-doped ZnS hollow spheres with enhanced UV and visible-light photocatalytic H2-production activity. Journal of Materials Chemistry, 2011, 21, 14655.	6.7	203

#	Article	IF	CITATIONS
217	Fluorine ions-mediated morphology control of anatase TiO2 with enhanced photocatalytic activity. Physical Chemistry Chemical Physics, 2012, 14, 5349.	2.8	203
218	Hydrothermal preparation and photocatalytic activity of mesoporous Au–TiO2 nanocomposite microspheres. Journal of Colloid and Interface Science, 2009, 334, 58-64.	9.4	200
219	Enhanced photovoltaic performance of dye-sensitized solar cells based on TiO2 nanosheets/graphene composite films. Journal of Materials Chemistry, 2012, 22, 17027.	6.7	200
220	Effects of pH on the microstructures and photocatalytic activity of mesoporous nanocrystalline titania powders prepared via hydrothermal method. Journal of Molecular Catalysis A, 2006, 258, 104-112.	4.8	199
221	Efficient catalytic removal of formaldehyde at room temperature using AlOOH nanoflakes with deposited Pt. Applied Catalysis B: Environmental, 2015, 163, 306-312.	20.2	199
222	TiO2/graphene composite photocatalysts for NOx removal: A comparison of surfactant-stabilized graphene and reduced graphene oxide. Applied Catalysis B: Environmental, 2016, 180, 637-647.	20.2	199
223	3D Grapheneâ€Based H <sub>2</sub> â€Production Photocatalyst and Electrocatalyst. Advanced Energy Materials, 2020, 10, 1903802.	19.5	199
224	Synthesis of Hierarchical Flower-like AlOOH and TiO <sub>2</sub> /AlOOH Superstructures and their Enhanced Photocatalytic Properties. Journal of Physical Chemistry C, 2009, 113, 17527-17535.	3.1	198
225	Dopamine Modified g-C <sub>3</sub> N <sub>4</sub> and Its Enhanced Visible-Light Photocatalytic H <sub>2</sub> -Production Activity. ACS Sustainable Chemistry and Engineering, 2018, 6, 8945-8953.	6.7	198
226	Nature-based catalyst for visible-light-driven photocatalytic CO <sub>2</sub> reduction. Energy and Environmental Science, 2018, 11, 2382-2389.	30.8	198
227	Nitrogen-doped TiO2 microsheets with enhanced visible light photocatalytic activity for CO2 reduction. Chinese Journal of Catalysis, 2015, 36, 2127-2134.	14.0	197
228	Room-temperature catalytic oxidation of formaldehyde on catalysts. Catalysis Science and Technology, 2016, 6, 3649-3669.	4.1	197
229	Enhanced Photoinduced-Stability and Photocatalytic Activity of CdS by Dual Amorphous Cocatalysts: Synergistic Effect of Ti(IV)-Hole Cocatalyst and Ni(II)-Electron Cocatalyst. Journal of Physical Chemistry C, 2016, 120, 3722-3730.	3.1	195
230	Synthesis of Boehmite Hollow Core/Shell and Hollow Microspheres via Sodium Tartrate-Mediated Phase Transformation and Their Enhanced Adsorption Performance in Water Treatment. Journal of Physical Chemistry C, 2009, 113, 14739-14746.	3.1	194
231	Novel hollow microspheres of hierarchical zinc–aluminum layered double hydroxides and their enhanced adsorption capacity for phosphate in water. Journal of Hazardous Materials, 2011, 192, 1114-1121.	12.4	194
232	Efficient Removal of Formaldehyde by Nanosized Gold on Well-Defined CeO <sub>2</sub> Nanorods at Room Temperature. Environmental Science & Technology, 2014, 48, 9702-9708.	10.0	194
233	Single crystal CdS nanowires with high visible-light photocatalytic H2-production performance. Journal of Materials Chemistry A, 2013, 1, 10927.	10.3	193

Review on DFT calculation of <i>s</i>å€triazineâ€based carbon nitride., 2019, 1, 32-56.

#	Article	IF	CITATIONS
235	Hierarchically porous MnO2 microspheres with enhanced adsorption performance. Journal of Materials Chemistry A, 2013, 1, 11682.	10.3	192
236	Shape-dependent photocatalytic hydrogen evolution activity over a Pt nanoparticle coupled g-C <sub>3</sub> N <sub>4</sub> photocatalyst. Physical Chemistry Chemical Physics, 2016, 18, 19457-19463.	2.8	190
237	1D/2D TiO <sub>2</sub> /MoS <sub>2</sub> Hybrid Nanostructures for Enhanced Photocatalytic CO <sub>2</sub> Reduction. Advanced Optical Materials, 2018, 6, 1800911.	7.3	190
238	Highly Selective CO2 Capture and Its Direct Photochemical Conversion on Ordered 2D/1D Heterojunctions. Joule, 2019, 3, 2792-2805.	24.0	189
239	Hierarchically CdS–Ag2S nanocomposites for efficient photocatalytic H2 production. Applied Surface Science, 2019, 470, 196-204.	6.1	189
240	Enhancement in the photocatalytic H2 production activity of CdS NRs by Ag2S and NiS dual cocatalysts. Applied Catalysis B: Environmental, 2021, 288, 119994.	20.2	189
241	Effects of calcination temperatures on photocatalytic activity of SnO2/TiO2 composite films prepared by an EPD method. Journal of Hazardous Materials, 2008, 154, 1141-1148.	12.4	188
242	Mechanistic insight into the enhanced photocatalytic activity of single-atom Pt, Pd or Au-embedded g-C 3 N 4. Applied Surface Science, 2018, 433, 1175-1183.	6.1	188
243	Degradation of organics in reverse osmosis concentrate by electro-Fenton process. Journal of Hazardous Materials, 2012, 215-216, 287-293.	12.4	186
244	Visible-light-induced photoelectrochemical behaviors of Fe-modified TiO2 nanotube arrays. Nanoscale, 2011, 3, 3138.	5.6	183
245	Preparation and photocatalytic activity of mesoporous anatase TiO2 nanofibers by a hydrothermal method. Journal of Photochemistry and Photobiology A: Chemistry, 2006, 182, 121-127.	3.9	181
246	Visibleâ€Light Photocatalytic Activity and Deactivation Mechanism of Ag <sub>3</sub> PO <sub>4</sub> Spherical Particles. Chemistry - an Asian Journal, 2012, 7, 1902-1908.	3.3	181
247	Preparation and characterization of super-hydrophilic porous TiO2 coating films. Materials Chemistry and Physics, 2001, 68, 253-259.	4.0	180
248	Carbon-based two-dimensional layered materials for photocatalytic CO 2 reduction to solar fuels. Energy Storage Materials, 2016, 3, 24-35.	18.0	178
249	Spontaneous Formation of a Tungsten Trioxide Sphereâ€inâ€Shell Superstructure by Chemically Induced Selfâ€Transformation. Small, 2008, 4, 87-91.	10.0	176
250	Unique photocatalytic oxidation reactivity and selectivity of TiO2–graphene nanocomposites. Nanoscale, 2012, 4, 3193.	5.6	176
251	A Novel Electro-Fenton Process with H <sub>2</sub> O <sub>2</sub> Generation in a Rotating Disk Reactor for Organic Pollutant Degradation. Environmental Science and Technology Letters, 2014, 1, 320-324.	8.7	176
252	Hierarchical porous C/MnO <sub>2</sub> composite hollow microspheres with enhanced supercapacitor performance. Journal of Materials Chemistry A, 2017, 5, 8635-8643.	10.3	174

#	Article	IF	CITATIONS
253	Hierarchical NiS/N-doped carbon composite hollow spheres with excellent supercapacitor performance. Journal of Materials Chemistry A, 2017, 5, 21257-21265.	10.3	174
254	Triethylamine gas sensor based on Pt-functionalized hierarchical ZnO microspheres. Sensors and Actuators B: Chemical, 2021, 331, 129425.	7.8	174
255	Enhancing effects of water content and ultrasonic irradiation on the photocatalytic activity of nano-sized TiO2 powders. Journal of Photochemistry and Photobiology A: Chemistry, 2002, 148, 263-271.	3.9	173
256	Facile synthesis of novel hierarchical graphene–Bi2O2CO3 composites with enhanced photocatalytic performance under visible light. Dalton Transactions, 2012, 41, 14345.	3.3	172
257	Effect of substrates on the photocatalytic activity of nanometer TiO2 thin films. Materials Research Bulletin, 2000, 35, 1293-1301.	5.2	171
258	Highly Active Mesoporous Ferrihydrite Supported Pt Catalyst for Formaldehyde Removal at Room Temperature. Environmental Science & Technology, 2015, 49, 6637-6644.	10.0	171
259	Enhanced charge transfer kinetics of Fe2O3/CdS composite nanorod arrays using cobalt-phosphate as cocatalyst. Applied Catalysis B: Environmental, 2017, 218, 570-580.	20.2	171
260	Review on design and evaluation of environmental photocatalysts. Frontiers of Environmental Science and Engineering, 2018, 12, 1.	6.0	170
261	Enhanced photocatalytic activity of bimodal mesoporous titania powders by C60 modification. Dalton Transactions, 2011, 40, 6635.	3.3	169
262	Au/PtO nanoparticle-modified g-C 3 N 4 for plasmon-enhanced photocatalytic hydrogen evolution under visible light. Journal of Colloid and Interface Science, 2016, 461, 56-63.	9.4	169
263	Formaldehyde and volatile organic compound (VOC) emissions from particleboard: Identification of odorous compounds and effects of heat treatment. Building and Environment, 2017, 117, 118-126.	6.9	169
264	Hierarchical flower-like nickel(II) oxide microspheres with high adsorption capacity of Congo red in water. Journal of Colloid and Interface Science, 2017, 504, 688-696.	9.4	167
265	Enhanced Photocatalytic H <sub>2</sub> -Production Activity of g-C <sub>3</sub> N <sub>4</sub> Nanosheets via Optimal Photodeposition of Pt as Cocatalyst. ACS Sustainable Chemistry and Engineering, 2018, 6, 10472-10480.	6.7	166
266	A Single Cu-Center Containing Enzyme-Mimic Enabling Full Photosynthesis under CO <sub>2</sub> Reduction. ACS Nano, 2020, 14, 8584-8593.	14.6	166
267	Hierarchically Porous ZnO/g-C <sub>3</sub> N <sub>4</sub> S-Scheme Heterojunction Photocatalyst for Efficient H <sub>2</sub> O <sub>2</sub> Production. Langmuir, 2021, 37, 14114-14124.	3.5	165
268	Enhanced Visibleâ€Light Photocatalytic H <sub>2</sub> Production by Zn <sub><i>x</i></sub> Cd <sub>1â^'<i>x</i></sub> S Modified with Earthâ€Abundant Nickelâ€Based Cocatalysts. ChemSusChem, 2014, 7, 3426-3434.	6.8	164
269	High-surface area mesoporous Pt/TiO 2 hollow chains for efficient formaldehyde decomposition at ambient temperature. Journal of Hazardous Materials, 2016, 301, 522-530.	12.4	162
270	Effects of Trifluoroacetic Acid Modification on the Surface Microstructures and Photocatalytic Activity of Mesoporous TiO2Thin Films. Langmuir, 2003, 19, 3889-3896.	3.5	160

#	Article	IF	CITATIONS
271	Construction of nickel cobalt sulfide nanosheet arrays on carbon cloth for performance-enhanced supercapacitor. Journal of Materials Science and Technology, 2020, 47, 113-121.	10.7	160
272	Fluorinated semiconductor photocatalysts: Tunable synthesis and unique properties. Advances in Colloid and Interface Science, 2012, 173, 35-53.	14.7	159
273	Photocatalytic water splitting for hydrogen generation on cubic, orthorhombic, and tetragonal KNbO3 microcubes. Nanoscale, 2013, 5, 8375.	5.6	159
274	Near-infrared absorbing 2D/3D ZnIn2S4/N-doped graphene photocatalyst for highly efficient CO2 capture and photocatalytic reduction. Science China Materials, 2020, 63, 552-565.	6.3	159
275	Sustained CO2-photoreduction activity and high selectivity over Mn, C-codoped ZnO core-triple shell hollow spheres. Nature Communications, 2021, 12, 4936.	12.8	159
276	A Simple and General Method for the Synthesis of Multicomponent Na2V6O16·3H2O Single-Crystal Nanobelts. Journal of the American Chemical Society, 2004, 126, 3422-3423.	13.7	158
277	Synthesis of reduced graphene oxide supported nickel-cobalt-layered double hydroxide nanosheets for supercapacitors. Journal of Colloid and Interface Science, 2021, 588, 637-645.	9.4	156
278	Optimizing Atomic Hydrogen Desorption of Sulfurâ€Rich NiS <sub>1+</sub> <i><sub>x</sub></i> Cocatalyst for Boosting Photocatalytic H <sub>2</sub> Evolution. Advanced Materials, 2022, 34, e2108475.	21.0	156
279	Title is missing!. Journal of Sol-Gel Science and Technology, 2000, 17, 163-171.	2.4	154
280	Preparation, characterization and photocatalytic activity of in situ Fe-doped TiO2 thin films. Thin Solid Films, 2006, 496, 273-280.	1.8	154
281	Noble-metal-free carbon nanotube-Cd0.1Zn0.9S composites for high visible-light photocatalytic H2-production performance. Nanoscale, 2012, 4, 2670.	5.6	154
282	Hierarchical flower-like C/NiO composite hollow microspheres and its excellent supercapacitor performance. Journal of Power Sources, 2017, 359, 371-378.	7.8	154
283	Photocatalytic activity of Ag <sub>2</sub> MO <sub>4</sub> (M = Cr, Mo, W) photocatalysts. Journal of Materials Chemistry A, 2015, 3, 20153-20166.	10.3	152
284	Improving photoanodes to obtain highly efficient dye-sensitized solar cells: a brief review. Materials Horizons, 2017, 4, 319-344.	12.2	152
285	Inorganic Metalâ€Oxide Photocatalyst for H <sub>2</sub> O <sub>2</sub> Production. Small, 2022, 18, e2104561.	10.0	152
286	The new understanding on photocatalytic mechanism of visible-light response NS codoped anatase TiO2 by first-principles. Applied Catalysis B: Environmental, 2013, 142-143, 45-53.	20.2	151
287	Hierarchical honeycomb-like Pt/NiFe-LDH/rGO nanocomposite with excellent formaldehyde decomposition activity. Chemical Engineering Journal, 2019, 365, 378-388.	12.7	151
288	Ultrahigh yield of hydrogen peroxide on graphite felt cathode modified with electrochemically exfoliated graphene. Journal of Materials Chemistry A, 2017, 5, 8070-8080.	10.3	150

#	Article	IF	CITATIONS
289	0D/2D NiS2/V-MXene composite for electrocatalytic H2 evolution. Journal of Catalysis, 2019, 375, 8-20.	6.2	150
290	Synthesis and Enhanced Photocatalytic Activity of a Hierarchical Porous Flowerlike <i>p–n</i> Junction NiO/TiO <sub>2</sub> Photocatalyst. Chemistry - an Asian Journal, 2010, 5, 2499-2506.	3.3	149
291	NaOH-Modified Ceramic Honeycomb with Enhanced Formaldehyde Adsorption and Removal Performance. Environmental Science & Technology, 2013, 47, 9928-9933.	10.0	149
292	Enhanced Photocatalytic Hydrogenâ€Production Performance of Graphene–Zn <sub><i>x</i></sub> Cd <sub>1â^'<i>x</i></sub> S Composites by Using an Organic S Source. Chemistry - A European Journal, 2014, 20, 1176-1185.	3.3	149
293	New insight into the enhanced visible-light photocatalytic activities of B-, C- and B/C-doped anatase TiO2 by first-principles. Physical Chemistry Chemical Physics, 2013, 15, 12040.	2.8	148
294	Highly efficient TiO <sub>2</sub> single-crystal photocatalyst with spatially separated Ag and F <sup>â^²</sup> bi-cocatalysts: orientation transfer of photogenerated charges and their rapid interfacial reaction. Journal of Materials Chemistry A, 2016, 4, 8682-8689.	10.3	148
295	Hybrid 0D–2D black phosphorus quantum dots–graphitic carbon nitride nanosheets for efficient hydrogen evolution. Nano Energy, 2018, 50, 552-561.	16.0	148
296	The pulsed laser-induced Schottky junction via in-situ forming Cd clusters on CdS surfaces toward efficient visible light-driven photocatalytic hydrogen evolution. Applied Catalysis B: Environmental, 2019, 258, 117967.	20.2	148
297	Review on nickel-based adsorption materials for Congo red. Journal of Hazardous Materials, 2021, 403, 123559.	12.4	148
298	Ionicâ€Liquidâ€Assisted Synthesis of Uniform Fluorinated B/Câ€Codoped TiO <sub>2</sub> Nanocrystals and Their Enhanced Visibleâ€Light Photocatalytic Activity. Chemistry - A European Journal, 2013, 19, 2433-2441.	3.3	147
299	Three-dimensional carbon foam supported MnO2/Pt for rapid capture and catalytic oxidation of formaldehyde at room temperature. Applied Catalysis B: Environmental, 2020, 267, 118689.	20.2	147
300	Facile fabrication of mesoporous MgO microspheres and their enhanced adsorption performance for phosphate from aqueous solutions. Colloids and Surfaces A: Physicochemical and Engineering Aspects, 2011, 379, 102-108.	4.7	146
301	Advances in bioleaching for recovery of metals and bioremediation of fuel ash and sewage sludge. Bioresource Technology, 2018, 261, 428-440.	9.6	146
302	A flexible bio-inspired H2-production photocatalyst. Applied Catalysis B: Environmental, 2018, 220, 148-160.	20.2	146
303	ZnO hierarchical microsphere for enhanced photocatalytic activity. Journal of Alloys and Compounds, 2018, 741, 622-632.	5.5	145
304	MOFâ€Based Transparent Passivation Layer Modified ZnO Nanorod Arrays for Enhanced Photoâ€Electrochemical Water Splitting. Advanced Energy Materials, 2018, 8, 1800101.	19.5	143
305	Enhanced formaldehyde oxidation on CeO 2 /AlOOH-supported Pt catalyst at room temperature. Applied Catalysis B: Environmental, 2016, 199, 458-465.	20.2	142
306	A facile hydrothermal synthesis of carbon dots modified g-C <sub>3</sub> N <sub>4</sub> for enhanced photocatalytic H <sub>2</sub> -evolution performance. Dalton Transactions, 2017, 46, 6417-6424.	3.3	142

#	Article	IF	CITATIONS
307	Fabrication of a hierarchical NiO/C hollow sphere composite and its enhanced supercapacitor performance. Chemical Communications, 2018, 54, 3731-3734.	4.1	140
308	Dye-Sensitization-Induced Visible-Light Reduction of Graphene Oxide for the Enhanced TiO <sub>2</sub> Photocatalytic Performance. ACS Applied Materials & Interfaces, 2013, 5, 2924-2929.	8.0	139
309	Effects of PAA additive and temperature on morphology of calcium carbonate particles. Journal of Solid State Chemistry, 2004, 177, 681-689.	2.9	138
310	Cu2(OH)2CO3 clusters: Novel noble-metal-free cocatalysts for efficient photocatalytic hydrogen production from water splitting. Applied Catalysis B: Environmental, 2017, 205, 104-111.	20.2	137
311	Rapid synthesis of mesoporous TiO2 with high photocatalytic activity by ultrasound-induced agglomeration. New Journal of Chemistry, 2002, 26, 416-420.	2.8	136
312	Facile Hydrothermal Synthesis of Hierarchical Boehmite: Sulfate-Mediated Transformation from Nanoflakes to Hollow Microspheres. Crystal Growth and Design, 2010, 10, 3977-3982.	3.0	136
313	Enhanced photocatalytic H2-production activity of bicomponent NiO/TiO2 composite nanofibers. Journal of Colloid and Interface Science, 2015, 449, 115-121.	9.4	136
314	Few-Layered Graphene-like Boron Nitride: A Highly Efficient Adsorbent for Indoor Formaldehyde Removal. Environmental Science and Technology Letters, 2017, 4, 20-25.	8.7	136
315	Adsorption investigation of CO2 on g-C3N4 surface by DFT calculation. Journal of CO2 Utilization, 2017, 21, 327-335.	6.8	134
316	Effect of surface treatment on the photocatalytic activity and hydrophilic property of the sol-gel derived TiO2 thin films. Materials Research Bulletin, 2001, 36, 97-107.	5.2	133
317	Hierarchical NiO–SiO2 composite hollow microspheres with enhanced adsorption affinity towards Congo red in water. Journal of Colloid and Interface Science, 2016, 466, 238-246.	9.4	133
318	Template-free fabrication of hierarchically flower-like tungsten trioxide assemblies with enhanced visible-light-driven photocatalytic activity. Journal of Hazardous Materials, 2009, 169, 221-227.	12.4	132
319	Preparation and adsorption performance of cross-linked porous polycarbazoles. Journal of Materials Chemistry A, 2014, 2, 16181-16189.	10.3	132
320	NH4Cl-induced low-temperature formation of nitrogen-rich g-C3N4 nanosheets with improved photocatalytic hydrogen evolution. Carbon, 2019, 153, 757-766.	10.3	132
321	Light-induced super-hydrophilicity and photocatalytic activity of mesoporous TiO2 thin films. Journal of Photochemistry and Photobiology A: Chemistry, 2002, 148, 331-339.	3.9	131
322	Effects of hydrothermal post-treatment on microstructures and morphology of titanate nanoribbons. Journal of Solid State Chemistry, 2006, 179, 349-354.	2.9	131
323	Cooperative self-construction and enhanced optical absorption of nanoplates-assembled hierarchical Bi2WO6 flowers. Journal of Solid State Chemistry, 2008, 181, 1048-1055.	2.9	131
324	Development of multifunctional photoactive self-cleaning glasses. Journal of Non-Crystalline Solids, 2008, 354, 1424-1430.	3.1	130

#	Article	IF	CITATIONS
325	Enhanced photoinduced stability and photocatalytic activity of AgBr photocatalyst by surface modification of Fe(III) cocatalyst. Applied Catalysis B: Environmental, 2014, 144, 75-82.	20.2	130
326	Oxidation of Rhodamine B by persulfate activated with porous carbon aerogel through a non-radical mechanism. Journal of Hazardous Materials, 2018, 358, 53-61.	12.4	130
327	Ultrasonic preparation of mesoporous titanium dioxide nanocrystalline photocatalysts and evaluation of photocatalytic activity. Journal of Molecular Catalysis A, 2005, 227, 75-80.	4.8	128
328	Preparation and enhanced daylight-induced photocatalytic activity of C,N,S-tridoped titanium dioxide powders. Journal of Hazardous Materials, 2008, 152, 1229-1236.	12.4	128
329	Amine-Functionalized Titanate Nanosheet-Assembled Yolk@Shell Microspheres for Efficient Cocatalyst-Free Visible-Light Photocatalytic CO <sub>2</sub> Reduction. ACS Applied Materials & Interfaces, 2015, 7, 8166-8175.	8.0	128
330	Enhanced visible-light photocatalytic H <sub>2</sub> -generation activity of carbon/g-C <sub>3</sub> N <sub>4</sub> nanocomposites prepared by two-step thermal treatment. Dalton Transactions, 2017, 46, 10611-10619.	3.3	128
331	The effect of Fâ^'-doping and temperature on the structural and textural evolution of mesoporous TiO2 powders. Journal of Solid State Chemistry, 2003, 174, 372-380.	2.9	127
332	Dye-sensitized solar cells based on hollow anatase TiO2 spheres prepared by self-transformation method. Electrochimica Acta, 2010, 55, 597-602.	5.2	127
333	Enhancing photocatalytic activity of one-dimensional KNbO3 nanowires by Au nanoparticles under ultraviolet and visible-light. Nanoscale, 2011, 3, 5161.	5.6	127
334	Cr(VI) removal from aqueous solutions by hydrothermal synthetic layered double hydroxides: Adsorption performance, coexisting anions and regeneration studies. Colloids and Surfaces A: Physicochemical and Engineering Aspects, 2014, 457, 33-40.	4.7	127
335	gâ€C <sub>3</sub> N <sub>4</sub> â€Based 2D/2D Composite Heterojunction Photocatalyst. Small Structures, 2021, 2, 2100086.	12.0	127
336	Fabrication and CO2 adsorption performance of bimodal porous silica hollow spheres with amine-modified surfaces. RSC Advances, 2012, 2, 6784.	3.6	125
337	Rattle-type Carbon–Alumina Core–Shell Spheres: Synthesis and Application for Adsorption of Organic Dyes. ACS Applied Materials & Interfaces, 2012, 4, 2174-2179.	8.0	124
338	Halogen poisoning effect of Pt-TiO2 for formaldehyde catalytic oxidation performance at room temperature. Applied Surface Science, 2016, 364, 808-814.	6.1	124
339	Enhanced Photocatalytic H <sub>2</sub> â€Production Activity of CdS Quantum Dots Using Sn <sup>2+</sup> as Cocatalyst under Visible Light Irradiation. Small, 2020, 16, e2001024.	10.0	124
340	Synthesis of amino-functionalized mesoporous alumina with enhanced affinity towards Cr(VI) and CO2. Chemical Engineering Journal, 2014, 239, 207-215.	12.7	123
341	Hierarchical C/NiO-ZnO nanocomposite fibers with enhanced adsorption capacity for Congo red. Journal of Colloid and Interface Science, 2019, 537, 736-745.	9.4	123
342	Hierarchically Macro-Mesoporous Pt/γ-Al2O3 Composite Microspheres for Efficient Formaldehyde Oxidation at Room Temperature. Scientific Reports, 2013, 3, 3215.	3.3	122

#	Article	IF	CITATIONS
343	Phenylamine-Functionalized rGO/TiO <sub>2</sub> Photocatalysts: Spatially Separated Adsorption Sites and Tunable Photocatalytic Selectivity. ACS Applied Materials & Interfaces, 2016, 8, 29470-29477.	8.0	122
344	Iron-based persulfate activation process for environmental decontamination in water and soil. Chemosphere, 2021, 265, 129057.	8.2	122
345	Synthesis and adsorption performance of Mg(OH)2 hexagonal nanosheet–graphene oxide composites. Applied Surface Science, 2015, 332, 121-129.	6.1	121
346	Effects of alcohol content and calcination temperature on the textural properties of bimodally mesoporous titania. Applied Catalysis A: General, 2003, 255, 309-320.	4.3	117
347	Dye-sensitized solar cells based on double-layered TiO2 composite films and enhanced photovoltaic performance. Electrochimica Acta, 2011, 56, 6293-6298.	5.2	117
348	Step-by-Step Mechanism Insights into the TiO <sub>2</sub> /Ce <sub>2</sub> S <sub>3</sub> S-Scheme Photocatalyst for Enhanced Aniline Production with Water as a Proton Source. ACS Catalysis, 2022, 12, 164-172.	11.2	117
349	Graphdiyne: a superior carbon additive to boost the activity of water oxidation catalysts. Nanoscale Horizons, 2018, 3, 317-326.	8.0	116
350	Enhanced removal of antibiotics from secondary wastewater effluents by novel UV/pre-magnetized Fe0/H2O2 process. Water Research, 2019, 153, 144-159.	11.3	115
351	Tandem photocatalytic oxidation of Rhodamine B over surface fluorinated bismuth vanadate crystals. Journal of Materials Chemistry, 2012, 22, 17759.	6.7	114
352	New Co(OH) <sub>2</sub> /CdS nanowires for efficient visible light photocatalytic hydrogen production. Journal of Materials Chemistry A, 2016, 4, 5282-5287.	10.3	114
353	Adsorption of N719 Dye on Anatase TiO <sub>2</sub> Nanoparticles and Nanosheets with Exposed (001) Facets: Equilibrium, Kinetic, and Thermodynamic Studies. Chemistry - an Asian Journal, 2011, 6, 2481-2490.	3.3	113
354	Enhanced photocatalytic CO <sub>2</sub> valorization over TiO <sub>2</sub> hollow microspheres by synergetic surface tailoring and Au decoration. Journal of Materials Chemistry A, 2018, 6, 24245-24255.	10.3	113
355	EPR Investigation on Electron Transfer of 2D/3D gâ€C <sub>3</sub> N <sub>4</sub> /ZnO Sâ€Scheme Heterojunction for Enhanced CO <sub>2</sub> Photoreduction. Advanced Sustainable Systems, 2022, 6, 2100264.	5.3	112
356	Enhanced photocatalytic performance of Ag3PO4 by simutaneous loading of Ag nanoparticles and Fe(III) cocatalyst. Applied Catalysis B: Environmental, 2014, 160-161, 658-665.	20.2	110
357	Suspensible Cubic-Phase CdS Nanocrystal Photocatalyst: Facile Synthesis and Highly Efficient H <sub>2</sub> -Evolution Performance in a Sulfur-Rich System. ACS Sustainable Chemistry and Engineering, 2018, 6, 5513-5523.	6.7	110
358	Carbon-modified Bi2WO6 nanostructures with improved photocatalytic activity under visible light. Dalton Transactions, 2010, 39, 3420.	3.3	109
359	Enhanced photocatalytic activity and photoinduced stability of Ag-based photocatalysts: The synergistic action of amorphous-Ti(IV) and Fe(III) cocatalysts. Applied Catalysis B: Environmental, 2016, 187, 163-170.	20.2	109
360	Preparation and characterization of visible-light-driven plasmonic photocatalyst Ag/AgCl/TiO2 nanocomposite thin films. Journal of Photochemistry and Photobiology A: Chemistry, 2011, 223, 82-87.	3.9	108

#	Article	IF	CITATIONS
361	Microemulsion-assisted synthesis of hierarchical porous Ni(OH)2/SiO2 composites toward efficient removal of formaldehyde in air. Dalton Transactions, 2013, 42, 10190.	3.3	108
362	Enhanced photoelectrocatalytic performance of SnO2/TiO2 rutile composite films. Journal of Materials Chemistry A, 2013, 1, 10727.	10.3	108
363	Enhanced visible light photocatalytic hydrogen production activity of CuS/ZnS nanoflower spheres. Journal of Materials Chemistry A, 2015, 3, 13913-13919.	10.3	108
364	S-scheme ZnO/WO3 heterojunction photocatalyst for efficient H2O2 production. Journal of Materials Science and Technology, 2022, 124, 193-201.	10.7	108
365	Synthesis, characterization and photocatalytic activity of mesoporous titania nanorod/titanate nanotube composites. Journal of Hazardous Materials, 2007, 147, 581-587.	12.4	107
366	Visibleâ€Light Photocatalytic Hydrogen Production Activity of ZnIn <sub>2</sub> S <sub>4</sub> Microspheres Using Carbon Quantum Dots and Platinum as Dual Coâ€catalysts. Chemistry - an Asian Journal, 2014, 9, 1766-1770.	3.3	107
367	High-yield lactic acid-mediated route for a g-C <sub>3</sub> N <sub>4</sub> nanosheet photocatalyst with enhanced H <sub>2</sub> -evolution performance. Nanoscale, 2019, 11, 9608-9616.	5.6	107
368	ZIF-67 derived nickel cobalt sulfide hollow cages for high-performance supercapacitors. Applied Surface Science, 2020, 504, 144501.	6.1	107
369	Highly efficient and stable FeIIFeIII LDH carbon felt cathode for removal of pharmaceutical ofloxacin at neutral pH. Journal of Hazardous Materials, 2020, 393, 122513.	12.4	107
370	Ag-Modified BiOCl Single-Crystal Nanosheets: Dependence of Photocatalytic Performance on the Region-Selective Deposition of Ag Nanoparticles. Journal of Physical Chemistry C, 2017, 121, 13191-13201.	3.1	106
371	Enhanced photocatalytic CO2 reduction activity of MOF-derived ZnO/NiO porous hollow spheres. Journal of CO2 Utilization, 2018, 24, 548-554.	6.8	106
372	Microwaveâ€Hydrothermal Preparation and Visibleâ€Light Photoactivity of Plasmonic Photocatalyst Agâ€TiO <sub>2</sub> Nanocomposite Hollow Spheres. Chemistry - an Asian Journal, 2010, 5, 1466-1474.	3.3	105
373	Enhanced photocatalytic CO2-reduction activity of electrospun mesoporous TiO2 nanofibers by solvothermal treatment. Dalton Transactions, 2014, 43, 9158.	3.3	105
374	Anchoring single Pt atoms and black phosphorene dual co-catalysts on CdS nanospheres to boost visible-light photocatalytic H2 evolution. Nano Today, 2021, 37, 101080.	11.9	105
375	Template-free hydrothermal fabrication of hierarchically organized γ-AlOOH hollow microspheres. Microporous and Mesoporous Materials, 2009, 122, 42-47.	4.4	103
376	Preparation of monodispersed cubic calcium carbonate particles via precipitation reaction. Materials Letters, 2004, 58, 1565-1570.	2.6	102
377	Microbial fuel cells for biosensor applications. Biotechnology Letters, 2015, 37, 2357-2364.	2.2	102
378	Solar fuel generation over nature-inspired recyclable TiO2/g-C3N4 S-scheme hierarchical thin-film photocatalyst. Journal of Materials Science and Technology, 2022, 112, 1-10.	10.7	101

#	Article	IF	CITATIONS
379	Sandwichâ€Shell Structured CoMn <sub>2</sub> O <sub>4</sub> /C Hollow Nanospheres for Performanceâ€Enhanced Sodiumâ€Ion Hybrid Supercapacitor. Advanced Energy Materials, 2022, 12, .	19.5	101
380	Additive-mediated intercalation and surface modification of MXenes. Chemical Society Reviews, 2022, 51, 2972-2990.	38.1	101
381	Enhanced visible-light photocatalytic H2-production performance of multi-armed CdS nanorods. RSC Advances, 2012, 2, 11829.	3.6	100
382	Microwave-assisted solvothermal synthesis of Bi4O5I2 hierarchical architectures with high photocatalytic performance. Catalysis Today, 2016, 264, 221-228.	4.4	100
383	Fabrication and enhanced CO2 reduction performance of N-self-doped TiO2 microsheet photocatalyst by bi-cocatalyst modification. Journal of CO2 Utilization, 2016, 16, 442-449.	6.8	99
384	In-situ growth of few-layer graphene on ZnO with intimate interfacial contact for enhanced photocatalytic CO2 reduction activity. Chemical Engineering Journal, 2021, 411, 128501.	12.7	99
385	Structural evidence of secondary phase segregation from the Raman vibrational modes in Zn1â^'xCoxOâ€^( <x<0.6). .<="" 2007,="" 91,="" applied="" letters,="" physics="" td=""><td>3.3</td><td>98</td></x<0.6).>	3.3	98
386	Hierarchical hollow cages of Mn-Co layered double hydroxide as supercapacitor electrode materials. Applied Surface Science, 2017, 413, 35-40.	6.1	98
387	Cooperatively modulating reactive oxygen species generation and bacteria-photocatalyst contact over graphitic carbon nitride by polyethylenimine for rapid water disinfection. Applied Catalysis B: Environmental, 2020, 274, 119095.	20.2	97
388	Reaction: Rational Design of Highly Active Photocatalysts for CO2 Conversion. CheM, 2020, 6, 1039-1040.	11.7	97
389	A high-response formaldehyde sensor based on fibrous Ag-ZnO/In2O3 with multi-level heterojunctions. Journal of Hazardous Materials, 2021, 413, 125352.	12.4	97
390	Title is missing!. Journal of Materials Science Letters, 2000, 19, 1015-1017.	0.5	96
391	Effect of calcination temperatures on microstructures and photocatalytic activity of tungsten trioxide hollow microspheres. Journal of Hazardous Materials, 2008, 160, 621-628.	12.4	96
392	Enhanced Photocalytic Activity of Hollow Anatase Microspheres by Sn <sup>4+</sup> Incorporation. Journal of Physical Chemistry C, 2008, 112, 2050-2057.	3.1	96
393	Effects of annealing on the microstructures and photoactivity of fluorinated N-doped TiO2. Physical Chemistry Chemical Physics, 2010, 12, 12308.	2.8	96
394	Hypercrosslinked porous polycarbazoles via one-step oxidative coupling reaction and Friedel–Crafts alkylation. Polymer Chemistry, 2015, 6, 2478-2487.	3.9	96
395	BiOBr/NiO S cheme Heterojunction Photocatalyst for CO <sub>2</sub> Photoreduction. Solar Rrl, 2022, 6, 2100587.	5.8	96
396	Effect of PSS on morphology and optical properties of ZnO. Journal of Colloid and Interface Science, 2008, 326, 433-438.	9.4	95

#	Article	IF	CITATIONS
397	Bio-template-assisted synthesis of hierarchically hollow SiO2 microtubes and their enhanced formaldehyde adsorption performance. Applied Surface Science, 2013, 274, 110-116.	6.1	94
398	Photocatalytic activity of modified g-C 3 N 4 /TiO 2 nanocomposites for NOx removal. Catalysis Today, 2017, 280, 37-44.	4.4	94
399	TiO <sub>2</sub> Photonic Crystals with Localized Surface Photothermal Effect and Enhanced Photocatalytic CO <sub>2</sub> Reduction Activity. ACS Sustainable Chemistry and Engineering, 2018, 6, 15653-15661.	6.7	94
400	ZnO/COF S-scheme heterojunction for improved photocatalytic H2O2 production performance. Chemical Engineering Journal, 2022, 444, 136584.	12.7	94
401	Facile preparation of calcium carbonate particles with unusual morphologies by precipitation reaction. Journal of Crystal Growth, 2004, 261, 566-570.	1.5	93
402	Layered manganese oxides for formaldehyde-oxidation at room temperature: the effect of interlayer cations. RSC Advances, 2015, 5, 100434-100442.	3.6	92
403	CdS nanosheets decorated with Ni@graphene core-shell cocatalyst for superior photocatalytic H2 production. Journal of Materials Science and Technology, 2020, 56, 170-178.	10.7	92
404	CsPbBr <sub>3</sub> Nanocrystal Induced Bilateral Interface Modification for Efficient Planar Perovskite Solar Cells. Advanced Science, 2021, 8, e2102648.	11.2	92
405	Promoting intramolecular charge transfer of graphitic carbon nitride by donor–acceptor modulation for visibleâ€light photocatalytic H <sub>2</sub> evolution. , 2022, 1, 294-308.		92
406	Characterization of mesoporous nanocrystalline TiO2 photocatalysts synthesized via a sol-solvothermal process at a low temperature. Journal of Solid State Chemistry, 2005, 178, 321-328.	2.9	91
407	Hierarchically porous calcined lithium/aluminum layered double hydroxides: Facile synthesis and enhanced adsorption towards fluoride in water. Journal of Materials Chemistry, 2011, 21, 19353.	6.7	91
408	Preparation of thermally stable anatase TiO2 photocatalyst from TiOF2 precursor and its photocatalytic activity. Journal of Alloys and Compounds, 2011, 509, 4557-4562.	5.5	91
409	Thioether-Functionalized 2D Covalent Organic Framework Featuring Specific Affinity to Au for Photocatalytic Hydrogen Production from Seawater. ACS Sustainable Chemistry and Engineering, 2019, 7, 18574-18581.	6.7	91
410	Oneâ€Step Realization of Crystallization and Cyanoâ€Group Generation for gâ€C <sub>3</sub> N <sub>4</sub> Photocatalysts with Improved H <sub>2</sub> Production. Solar Rrl, 2021, 5, 2000372.	5.8	91
411	β-Cyclodextrin epichlorohydrin copolymer as a solid-phase extraction adsorbent for aromatic compounds in water samples. Analytica Chimica Acta, 2003, 477, 93-101.	5.4	90
412	Hierarchically structured functional materials: Synthesis strategies for multimodal porous networks. Pure and Applied Chemistry, 2009, 81, 2265-2307.	1.9	90
413	From Millimeter to Subnanometer: Vapor–Solid Deposition of Carbon Nitride Hierarchical Nanostructures Directed by Supramolecular Assembly. Angewandte Chemie - International Edition, 2017, 56, 8426-8430.	13.8	90
414	Binary Solvent Engineering for High-Performance Two-Dimensional Perovskite Solar Cells. ACS Sustainable Chemistry and Engineering, 2019, 7, 3487-3495.	6.7	90

#	Article	IF	CITATIONS
415	Comprehensive treatment of marine aquaculture wastewater by a cost-effective flow-through electro-oxidation process. Science of the Total Environment, 2020, 722, 137812.	8.0	90
416	Title is missing!. Journal of Materials Science Letters, 2001, 20, 1745-1748.	0.5	89
417	Effect of surface microstructure on the photoinduced hydrophilicity of porous TiO2 thin films. Journal of Materials Chemistry, 2002, 12, 81-85.	6.7	89
418	Dye-sensitized solar cells based on ordered titanate nanotube films fabricated by electrophoretic deposition method. Electrochemistry Communications, 2009, 11, 2052-2055.	4.7	89
419	Supramolecular Chemistry in Molten Sulfur: Preorganization Effects Leading to Marked Enhancement of Carbon Nitride Photoelectrochemistry. Advanced Functional Materials, 2015, 25, 6265-6271.	14.9	89
420	Origin of Tunable Photocatalytic Selectivity of Wellâ€Defined αâ€Fe <sub>2</sub> O <sub>3</sub> Nanocrystals. Small, 2014, 10, 674-679.	10.0	88
421	The dependence of photocatalytic activity and photoinduced self-stability of photosensitive Agl nanoparticles. Dalton Transactions, 2012, 41, 10405.	3.3	87
422	Flexible nickel foam decorated with Pt/NiO nanoflakes with oxygen vacancies for enhanced catalytic formaldehyde oxidation at room temperature. Environmental Science: Nano, 2017, 4, 2215-2224.	4.3	87
423	Enhanced solar-to-chemical energy conversion of graphitic carbon nitride by two-dimensional cocatalysts. EnergyChem, 2021, 3, 100051.	19.1	87
424	Microemulsionâ€Assisted Preparation of a Mesoporous Ferrihydrite/SiO <sub>2</sub> Composite for the Efficient Removal of Formaldehyde from Air. Chemistry - A European Journal, 2013, 19, 9592-9598.	3.3	86
425	Enhanced catalytic activity of hierarchically macro-/mesoporous Pt/TiO <sub>2</sub> toward room-temperature decomposition of formaldehyde. Catalysis Science and Technology, 2015, 5, 2366-2377.	4.1	86
426	Dual Z-scheme charge transfer in TiO2–Ag–Cu2O composite for enhanced photocatalytic hydrogen generation. Journal of Materiomics, 2015, 1, 124-133.	5.7	86
427	Direct Photoinduced Synthesis of Amorphous CoMoS <sub><i>x</i></sub> Cocatalyst and Its Improved Photocatalytic H <sub>2</sub> -Evolution Activity of CdS. ACS Sustainable Chemistry and Engineering, 2018, 6, 12436-12445.	6.7	86
428	In-situ preparation of TiO2/N-doped graphene hollow sphere photocatalyst with enhanced photocatalytic CO2 reduction performance. Chinese Journal of Catalysis, 2021, 42, 1648-1658.	14.0	86
429	Recent Advances in Morphology Control and Surface Modification of Bi-Based Photocatalysts. Wuli Huaxue Xuebao/ Acta Physico - Chimica Sinica, 2016, 32, 2841-2870.	4.9	85
430	TiO2/In2S3 S-scheme photocatalyst with enhanced H2O2-production activity. Nano Research, 2023, 16, 4506-4514.	10.4	85
431	A carbon nanotube-confined iron modified cathode with prominent stability and activity for heterogeneous electro-Fenton reactions. Journal of Materials Chemistry A, 2019, 7, 24408-24419.	10.3	84
432	Nearâ€Infraredâ€Responsive Photocatalysts. Small Methods, 2021, 5, e2001042.	8.6	84

#	Article	IF	CITATIONS
433	Photocatalytic activity of dispersed TiO2 particles deposited on glass fibers. Journal of Molecular Catalysis A, 2006, 246, 206-211.	4.8	83
434	Controlled synthesis of highly dispersed TiO2 nanoparticles using SBA-15 as hard template. Journal of Colloid and Interface Science, 2006, 304, 84-91.	9.4	83
435	Hierarchically nanostructured porous TiO2(B) with superior photocatalytic CO2 reduction activity. Science China Chemistry, 2018, 61, 344-350.	8.2	83
436	Rationally designed hierarchical NiCo2O4–C@Ni(OH)2 core-shell nanofibers for high performance supercapacitors. Carbon, 2019, 152, 652-660.	10.3	83
437	Quenching induced hierarchical 3D porous g-C <sub>3</sub> N <sub>4</sub> with enhanced photocatalytic CO <sub>2</sub> reduction activity. Chemical Communications, 2019, 55, 14023-14026.	4.1	83
438	Controlling defects in crystalline carbon nitride to optimize photocatalytic CO <sub>2</sub> reduction. Chemical Communications, 2020, 56, 5641-5644.	4.1	83
439	Synthesis of MgNiCo LDH hollow structure derived from ZIF-67 as superb adsorbent for Congo red. Journal of Colloid and Interface Science, 2022, 612, 598-607.	9.4	83
440	Synergetic Codoping in Fluorinated Ti <sub>1â^'<i>x</i></sub> Zr <sub><i>x</i></sub> O <sub>2</sub> Hollow Microspheres. Journal of Physical Chemistry C, 2009, 113, 10712-10717.	3.1	82
441	Photocatalytic Activity of Hierarchical Flower-Like TiO2 Superstructures with Dominant {001} Facets. Chinese Journal of Catalysis, 2011, 32, 525-531.	14.0	82
442	The Effect of SiO2 Addition on the Grain Size and Photocatalytic Activity of TiO2 Thin Films. Journal of Sol-Gel Science and Technology, 2002, 24, 95-103.	2.4	81
443	Ethyl acetate-induced formation of amorphous MoSx nanoclusters for improved H2-evolution activity of TiO2 photocatalyst. Chemical Engineering Journal, 2019, 375, 121934.	12.7	81
444	Simultaneous Realization of Direct Photoinduced Deposition and Improved H <sub>2</sub> -Evolution Performance of Sn-Nanoparticle-Modified TiO <sub>2</sub> Photocatalyst. ACS Sustainable Chemistry and Engineering, 2019, 7, 10084-10094.	6.7	81
445	Enhanced Photocatalytic Activity and Selectivity for CO <sub>2</sub> Reduction over a TiO <sub>2</sub> Nanofibre Mat Using Ag and MgO as Biâ€Cocatalyst. ChemCatChem, 2019, 11, 465-472.	3.7	81
446	Pt/C@MnO2 composite hierarchical hollow microspheres for catalytic formaldehyde decomposition at room temperature. Applied Surface Science, 2019, 466, 301-308.	6.1	81
447	Photocatalytic Activity and Characterization of the Sol-Gel Derived Pb-Doped TiO2 Thin Films. Journal of Sol-Gel Science and Technology, 2002, 24, 39-48.	2.4	80
448	In situ anion-exchange synthesis and photocatalytic activity of Ag8W4O16/AgCl-nanoparticle core–shell nanorods. Journal of Molecular Catalysis A, 2011, 334, 52-59.	4.8	80
449	Rolling-made gas diffusion electrode with carbon nanotube for electro-Fenton degradation of acetylsalicylic acid. Chemosphere, 2018, 206, 439-446.	8.2	80
450	Photocatalytic CO <sub>2</sub> reduction of C/ZnO nanofibers enhanced by an Ni-NiS cocatalyst. Nanoscale, 2020, 12, 7206-7213.	5.6	80

#	Article	IF	CITATIONS
451	Enhanced photocatalytic H <sub>2</sub> -production activity of TiO <sub>2</sub> using Ni(NO <sub>3</sub> ) <sub>2</sub> as an additive. Physical Chemistry Chemical Physics, 2013, 15, 12033-12039.	2.8	79
452	Simultaneous sulfadiazines degradation and disinfection from municipal secondary effluent by a flow-through electro-Fenton process with graphene-modified cathode. Journal of Hazardous Materials, 2019, 368, 830-839.	12.4	79
453	Zn Cd1–S quantum dot with enhanced photocatalytic H2-production performance. Chinese Journal of Catalysis, 2021, 42, 15-24.	14.0	79
454	Photocatalytic H <sub>2</sub> Evolution Coupled with Furfuralcohol Oxidation over Ptâ€Modified ZnCdS Solid Solution. Small Methods, 2021, 5, e2100979.	8.6	79
455	Preparation of high efficient photoelectrode of N–F-codoped TiO2 nanotubes. Journal of Photochemistry and Photobiology A: Chemistry, 2008, 194, 152-160.	3.9	78
456	Microemulsion-Assisted Synthesis of Mesoporous Aluminum Oxyhydroxide Nanoflakes for Efficient Removal of Gaseous Formaldehyde. ACS Applied Materials & Interfaces, 2014, 6, 2111-2117.	8.0	78
457	Hierarchical Pt/NiO Hollow Microspheres with Enhanced Catalytic Performance. ChemNanoMat, 2015, 1, 58-67.	2.8	78
458	Degradation and mechanism of 2,4-dichlorophenoxyacetic acid (2,4-D) by thermally activated persulfate oxidation. Chemosphere, 2018, 212, 784-793.	8.2	78
459	Enhanced photoinduced super-hydrophilicity of the sol–gel-derived TiO2 thin films by Fe-doping. Materials Chemistry and Physics, 2006, 95, 193-196.	4.0	77
460	Enhancement on the simultaneous removal of nitrate and organic pollutants from groundwater by a three-dimensional bio-electrochemical reactor. Bioresource Technology, 2009, 100, 4662-4668.	9.6	77
461	Tuning the strength of built-in electric field in 2D/2D g-C3N4/SnS2 and g-C3N4/ZrS2 S-scheme heterojunctions by nonmetal doping. Journal of Materiomics, 2021, 7, 988-997.	5.7	77
462	Effects of the preparation method on the structure and the visible-light photocatalytic activity of Ag <sub>2</sub> CrO <sub>4</sub> . Beilstein Journal of Nanotechnology, 2014, 5, 658-666.	2.8	76
463	Effect of microstructure and surface hydroxyls on the catalytic activity of Au/AlOOH for formaldehyde removal at room temperature. Journal of Colloid and Interface Science, 2017, 501, 164-174.	9.4	76
464	Enhanced Performance of Planar Perovskite Solar Cell by Graphene Quantum Dot Modification. ACS Sustainable Chemistry and Engineering, 2018, 6, 8631-8640.	6.7	76
465	Novel amorphous NiCuS H2-evolution cocatalyst: Optimizing surface hydrogen desorption for efficient photocatalytic activity. Chemical Engineering Journal, 2021, 419, 129652.	12.7	76
466	Crystalline phase-dependent photocatalytic water splitting for hydrogen generation on KNbO3 submicro-crystals. International Journal of Hydrogen Energy, 2013, 38, 3554-3561.	7.1	75
467	Ultrahigh-surface-area activated carbon aerogels derived from glucose for high-performance organic pollutants adsorption. Journal of Colloid and Interface Science, 2019, 546, 333-343.	9.4	75
468	S-Scheme 2D/2D Bi2MoO6/BiOI van der Waals heterojunction for CO2 photoreduction. Chinese Journal of Catalysis, 2022, 43, 1657-1666.	14.0	75

#	Article	IF	CITATIONS
469	3D BiOl–GO composite with enhanced photocatalytic performance for phenol degradation under visible-light. Ceramics International, 2015, 41, 3511-3517.	4.8	74
470	Room-temperature synthesis of BiOI with tailorable (0 0 1) facets and enhanced photocatalytic activity. Journal of Colloid and Interface Science, 2016, 478, 201-208.	9.4	74
471	Spontaneous construction of photoactive hollow TiO <sub>2</sub> microspheres and chains. Nanotechnology, 2009, 20, 325606.	2.6	73
472	Enhanced photocatalytic activity and stability of semiconductor by Ag doping and simultaneous deposition: the case of CdS. RSC Advances, 2013, 3, 20782.	3.6	73
473	Enhanced degradation of 2,4-dichlorophenoxyacetic acid by pre-magnetization Fe-C activated persulfate: Influential factors, mechanism and degradation pathway. Journal of Hazardous Materials, 2018, 353, 454-465.	12.4	73
474	Ni-P cluster modified carbon nitride toward efficient photocatalytic hydrogen production. Chinese Journal of Catalysis, 2019, 40, 867-874.	14.0	73
475	NiCo <sub>2</sub> S <sub>4</sub> Nanotubes Anchored 3D Nitrogen-Doped Graphene Framework as Electrode Material with Enhanced Performance for Asymmetric Supercapacitors. ACS Sustainable Chemistry and Engineering, 2019, 7, 11157-11165.	6.7	73
476	Controlled synthesis of calcium carbonate in a mixed aqueous solution of PSMA and CTAB. Journal of Solid State Chemistry, 2005, 178, 861-867.	2.9	72
477	A novel photoanode architecture of dye-sensitized solar cells based on TiO2 hollow sphere/nanorod array double-layer film. Journal of Colloid and Interface Science, 2012, 365, 46-52.	9.4	72
478	Hierarchically porous metastable β-Ag <sub>2</sub> WO <sub>4</sub> hollow nanospheres: controlled synthesis and high photocatalytic activity. Nanotechnology, 2013, 24, 165602.	2.6	72
479	Porous Fluorinated SnO <sub>2</sub> Hollow Nanospheres: Transformative Self-assembly and Photocatalytic Inactivation of Bacteria. ACS Applied Materials & Interfaces, 2014, 6, 2407-2414.	8.0	72
480	Hierarchically porous NiO–Al <sub>2</sub> O <sub>3</sub> nanocomposite with enhanced Congo red adsorption in water. RSC Advances, 2016, 6, 10272-10279.	3.6	72
481	Ni <i><sub>x</sub></i> S <i><sub>y</sub></i> Nanowalls/Nitrogenâ€Doped Graphene Foam Is an Efficient Trifunctional Catalyst for Unassisted Artificial Photosynthesis. Advanced Functional Materials, 2018, 28, 1706917.	14.9	72
482	Hollow CdS-based photocatalysts. Journal of Materiomics, 2021, 7, 419-439.	5.7	72
483	First-principles investigation of Cu-doped ZnS with enhanced photocatalytic hydrogen production activity. Chemical Physics Letters, 2017, 668, 1-6.	2.6	71
484	Analytical transmission electron microscopy for emerging advanced materials. Matter, 2021, 4, 2309-2339.	10.0	71
485	Hierarchical Pt/MnO <sub>2</sub> –Ni(OH) <sub>2</sub> Hybrid Nanoflakes with Enhanced Room-Temperature Formaldehyde Oxidation Activity. ACS Sustainable Chemistry and Engineering, 2018, 6, 12481-12488.	6.7	70
486	Intrinsic intermediate gap states of TiO2 materials and their roles in charge carrier kinetics. Journal of Photochemistry and Photobiology C: Photochemistry Reviews, 2019, 39, 1-57.	11.6	70

#	Article	IF	CITATIONS
487	Nickel-based cocatalysts for photocatalysis: Hydrogen evolution, overall water splitting and CO2 reduction. Materials Today Physics, 2020, 15, 100279.	6.0	70
488	Ice–Water Quenching Induced Ti <sup>3+</sup> Self-doped TiO <sub>2</sub> with Surface Lattice Distortion and the Increased Photocatalytic Activity. Journal of Physical Chemistry C, 2017, 121, 19836-19848.	3.1	69
489	Effect of phase structures on the formation rate of hydroxyl radicals on the surface of TiO2. Journal of Physics and Chemistry of Solids, 2010, 71, 519-522.	4.0	68
490	Effects of Adsorbed F, OH, and Cl Ions on Formaldehyde Adsorption Performance and Mechanism of Anatase TiO <sub>2</sub> Nanosheets with Exposed {001} Facets. ACS Applied Materials & Interfaces, 2013, 5, 8165-8172.	8.0	68
491	New Way for CO <sub>2</sub> Reduction under Visible Light by a Combination of a Cu Electrode and Semiconductor Thin Film: Cu <sub>2</sub> O Conduction Type and Morphology Effect. Journal of Physical Chemistry C, 2014, 118, 24467-24478.	3.1	68
492	Enhanced photocurrent density of HTM-free perovskite solar cells by carbon quantum dots. Applied Surface Science, 2018, 430, 625-631.	6.1	68
493	Synergistic effects of hollow structure and surface fluorination on the photocatalytic activity of titania. Journal of Hazardous Materials, 2010, 173, 539-543.	12.4	67
494	Enhancement of ethanol electrooxidation on plasmonic Au/TiO2 nanotube arrays. Electrochemistry Communications, 2011, 13, 1260-1263.	4.7	67
495	Amine-functionalized monodispersed porous silica microspheres with enhanced CO2 adsorption performance and good cyclic stability. Journal of Colloid and Interface Science, 2013, 408, 173-180.	9.4	67
496	Fabrication of carbon quantum dots and their application for efficient detecting Ru(bpy)32+ in the solution. Sensors and Actuators B: Chemical, 2013, 181, 209-214.	7.8	67
497	Effect of effective mass and spontaneous polarization on photocatalytic activity of wurtzite and zinc-blende ZnS. APL Materials, 2015, 3, .	5.1	67
498	Enhanced photocatalytic H2 production performance of CdS hollow spheres using C and Pt as bi-cocatalysts. Chinese Journal of Catalysis, 2021, 42, 743-752.	14.0	67
499	Tuning the photocatalytic selectivity of TiO2 anatase nanoplates by altering the exposed crystal facets content. Applied Catalysis B: Environmental, 2013, 142-143, 761-768.	20.2	66
500	Enhanced Visibleâ€Light Hydrogenâ€Production Activity of Copperâ€Modified Zn <sub><i>x</i></sub> Cd <sub>1â^'<i>x</i></sub> S. ChemSusChem, 2013, 6, 2009-2015.	6.8	66
501	Insights into the structure–photoreactivity relationships in well-defined perovskite ferroelectric KNbO <sub>3</sub> nanowires. Chemical Science, 2015, 6, 4118-4123.	7.4	66
502	Catalytic decomposition and mechanism of formaldehyde over Pt–Al <sub>2</sub> O <sub>3</sub> molecular sieves at room temperature. Physical Chemistry Chemical Physics, 2017, 19, 6957-6963.	2.8	66
503	Chestnut husk-like nickel cobaltite hollow microspheres for the adsorption of Congo red. Journal of Alloys and Compounds, 2018, 735, 1041-1051.	5.5	66
504	Synergistic Effect of Co(III) and Co(II) in a 3D Structured Co <sub>3</sub> O <sub>4</sub> /Carbon Felt Electrode for Enhanced Electrochemical Nitrate Reduction Reaction. ACS Applied Materials & Interfaces, 2021, 13, 28348-28358.	8.0	66

#	Article	IF	CITATIONS
505	Spontaneous Formation and Electrogenerated Chemiluminescence of Tris(bipyridine) Ru(II) Derivative Nanobelts. Journal of the American Chemical Society, 2008, 130, 7196-7197.	13.7	65
506	Influence of lattice integrity and phase composition on the photocatalytic hydrogen production efficiency of ZnS nanomaterials. Nanoscale, 2012, 4, 2859.	5.6	65
507	Cu(II) as a General Cocatalyst for Improved Visible-Light Photocatalytic Performance of Photosensitive Ag-Based Compounds. Journal of Physical Chemistry C, 2014, 118, 8891-8898.	3.1	65
508	Indirect electrochemical oxidation of 2,4-dichlorophenoxyacetic acid using electrochemically-generated persulfate. Chemosphere, 2018, 204, 163-169.	8.2	65
509	Plasmon-induced interfacial charge-transfer transition prompts enhanced CO2 photoreduction over Cu/Cu2O octahedrons. Chemical Engineering Journal, 2020, 397, 125390.	12.7	65
510	One-pot hydrothermal synthesis and enhanced photocatalytic activity of trifluoroacetic acid modified TiO2 hollow microspheres. Journal of Molecular Catalysis A, 2010, 326, 8-14.	4.8	64
511	Deactivation and regeneration of Pt/TiO2 nanosheet-type catalysts with exposed (001) facets for room temperature oxidation of formaldehyde. Journal of Molecular Catalysis A, 2014, 390, 7-13.	4.8	64
512	ZIF-8 derived bimodal carbon modified ZnO photocatalysts with enhanced photocatalytic CO <sub>2</sub> reduction performance. RSC Advances, 2016, 6, 59998-60006.	3.6	64
513	Room-temperature formaldehyde catalytic decomposition. Environmental Science: Nano, 2020, 7, 3655-3709.	4.3	64
514	A flow-through electro-Fenton process using modified activated carbon fiber cathode for orange II removal. Chemosphere, 2020, 252, 126483.	8.2	64
515	Enhanced room-temperature HCHO decomposition activity of highly-dispersed Pt/Al2O3 hierarchical microspheres with exposed {110} facets. Journal of Industrial and Engineering Chemistry, 2017, 45, 197-205.	5.8	63
516	Selective modification of ultra-thin g-C3N4 nanosheets on the (110) facet of Au/BiVO4 for boosting photocatalytic H2O2 production. Applied Catalysis B: Environmental, 2021, 297, 120414.	20.2	63
517	Bilayer hollow/spindle-like anatase TiO2 photoanode for high efficiency dye-sensitized solar cells. Journal of Power Sources, 2015, 278, 344-351.	7.8	62
518	Effect of calcination on adsorption performance of Mg–Al layered double hydroxide prepared by a water-in-oil microemulsion method. RSC Advances, 2016, 6, 50128-50137.	3.6	62
519	Hierarchical porous nickel supported NiFeOxHy nanosheets for efficient and robust oxygen evolution electrocatalyst under industrial condition. Applied Catalysis B: Environmental, 2021, 299, 120668.	20.2	62
520	Dynamics of Photogenerated Charge Carriers in Inorganic/Organic S-Scheme Heterojunctions. Journal of Physical Chemistry Letters, 2022, 13, 4695-4700.	4.6	62
521	Facile fabrication and characterization of hierarchically porous calcium carbonate microspheres. Chemical Communications, 2004, , 2414.	4.1	60
522	Selenium-enriched amorphous NiSe1+ nanoclusters as a highly efficient cocatalyst for photocatalytic H2 evolution. Chemical Engineering Journal, 2021, 408, 127230.	12.7	60

#	Article	IF	CITATIONS
523	Synthesis of Organized Layered Carbon by Selfâ€Templating of Dithiooxamide. Advanced Materials, 2016, 28, 6727-6733.	21.0	59
524	Cost-efficient improvement of coking wastewater biodegradability by multi-stages flow through peroxi-coagulation under low current load. Water Research, 2019, 154, 336-348.	11.3	59
525	Adsorption of CO2, O2, NO and CO on s-triazine-based g-C3N4 surface. Catalysis Today, 2019, 335, 117-127.	4.4	59
526	Improving Artificial Photosynthesis over Carbon Nitride by Gas–Liquid–Solid Interface Management for Full Lightâ€Induced CO <sub>2</sub> Reduction to C <sub>1</sub> and C <sub>2</sub> Fuels and O <sub>2</sub> . ChemSusChem, 2020, 13, 1730-1734.	6.8	59
527	Single-atom heterogeneous photocatalysts. Chem Catalysis, 2021, 1, 1173-1214.	6.1	59
528	Sonication assisted deposition of Cu2O nanoparticles on multiwall carbon nanotubes with polyol process. Carbon, 2005, 43, 670-673.	10.3	58
529	Spray-hydrolytic synthesis of highly photoactive mesoporous anatase nanospheres for the photocatalytic degradation of toluene in air. Applied Catalysis B: Environmental, 2009, 89, 160-166.	20.2	58
530	Synthesis of nanometer-size Bi3TaO7 and its visible-light photocatalytic activity for the degradation of a 4BS dye. Journal of Colloid and Interface Science, 2010, 345, 467-473.	9.4	58
531	Holey Graphene for Electrochemical Energy Storage. Cell Reports Physical Science, 2020, 1, 100215.	5.6	58
532	Pt–Ru Dimer Electrocatalyst with Electron Redistribution for Hydrogen Evolution Reaction. ACS Catalysis, 2022, 12, 5540-5548.	11.2	58
533	Effects of hierarchical structure on the performance of tin oxide-supported platinum catalyst for room-temperature formaldehyde oxidation. Chinese Journal of Catalysis, 2017, 38, 199-206.	14.0	57
534	Cobalt polyoxometalate on N-doped carbon layer to boost photoelectrochemical water oxidation of BiVO4. Chemical Engineering Journal, 2020, 392, 123744.	12.7	57
535	Hetero-phase MoC-Mo2C nanoparticles for enhanced photocatalytic H2-production activity of TiO2. Nano Research, 2021, 14, 1095-1102.	10.4	57
536	Recent advances in electro-Fenton process and its emerging applications. Critical Reviews in Environmental Science and Technology, 2023, 53, 887-913.	12.8	57
537	Novel preparation and photocatalytic activity of one-dimensional TiO2hollow structures. Nanotechnology, 2007, 18, 065604.	2.6	56
538	The effect of calcination temperature on the microstructure and photocatalytic activity of TiO2-based composite nanotubes prepared by an in situ template dissolution method. Nanoscale, 2012, 4, 6597.	5.6	56
539	High-efficiency dye-sensitized solar cells based on electrospun TiO2 multi-layered composite film photoanodes. Energy, 2015, 86, 196-203.	8.8	56
540	Highly efficient BiVO <sub>4</sub> single-crystal photocatalyst with selective Ag <sub>2</sub> O-Ag modification: orientation transport, rapid interfacial transfer and catalytic reaction. Dalton Transactions, 2018, 47, 6370-6377.	3.3	56

#	Article	IF	CITATIONS
541	Nanoconfined Nickel@Carbon Core–Shell Cocatalyst Promoting Highly Efficient Visibleâ€Light Photocatalytic H <sub>2</sub> Production. Small, 2018, 14, e1801705.	10.0	56
542	In Situ Synthesis of Mo <sub>2</sub> C Nanoparticles on Graphene Nanosheets for Enhanced Photocatalytic H <sub>2</sub> -Production Activity of TiO <sub>2</sub> . ACS Sustainable Chemistry and Engineering, 2021, 9, 3828-3837.	6.7	56
543	Effects of calcination temperature on microstructures and photocatalytic activity of titanate nanotube films prepared by an EPD method. Nanotechnology, 2008, 19, 045606.	2.6	54
544	Optical and photocatalytic properties of composite TiO2/ZnO thin films. Catalysis Today, 2014, 230, 174-180.	4.4	54
545	Solvothermal synthesis and photocatalytic performance of Mn 4+ -doped anatase nanoplates with exposed {0 0 1} facets. Applied Catalysis B: Environmental, 2015, 162, 27-33.	20.2	54
546	A photosynthetic algal microbial fuel cell for treating swine wastewater. Environmental Science and Pollution Research, 2019, 26, 6182-6190.	5.3	54
547	0D/2D (Fe0.5Ni0.5)S2/rGO nanocomposite with enhanced supercapacitor and lithium ion battery performance. Journal of Power Sources, 2019, 426, 266-274.	7.8	54
548	Carbon dioxide sequestration accompanied by bioenergy generation using a bubbling-type photosynthetic algae microbial fuel cell. Bioresource Technology, 2019, 280, 95-103.	9.6	54
549	Topotactic Transformation of Bismuth Oxybromide into Bismuth Tungstate: Bandgap Modulation of Single-Crystalline {001}-Faceted Nanosheets for Enhanced Photocatalytic CO <sub>2</sub> Reduction. ACS Applied Materials & Interfaces, 2020, 12, 26991-27000.	8.0	53
550	Triethanolamine-mediated photodeposition formation of amorphous Ni-P alloy for improved H2-evolution activity of g-C3N4. Science China Materials, 2020, 63, 2215-2227.	6.3	53
551	Facile synthesis and characterization of novel nanocomposites of titanate nanotubes and rutile nanocrystals. Materials Chemistry and Physics, 2006, 100, 507-512.	4.0	52
552	Photocatalytic activity of the calcined H-titanate nanowires for photocatalytic oxidation of acetone in air. Chemosphere, 2007, 66, 2050-2057.	8.2	52
553	Fabrication and photovoltaic performance of hierarchically titanate tubular structures self-assembled by nanotubes and nanosheets. Chemical Communications, 2011, 47, 9161.	4.1	52
554	Investigation of Al 2 O 3 and ZrO 2 spacer layers for fully printable and hole-conductor-free mesoscopic perovskite solar cells. Applied Surface Science, 2018, 430, 632-638.	6.1	52
555	Mesoporous TiO <sub>2</sub> Comprising Small, Highly Crystalline Nanoparticles for Efficient CO <sub>2</sub> Reduction by H <sub>2</sub> O. ACS Sustainable Chemistry and Engineering, 2018, 6, 531-540.	6.7	52
556	Enhanced photochemical CO <sub>2</sub> reduction in the gas phase by graphdiyne. Journal of Materials Chemistry A, 2020, 8, 7671-7676.	10.3	52
557	Bactericidal and photocatalytic activities of TiO2 thin films prepared by sol–gel and reverse micelle methods. Journal of Photochemistry and Photobiology A: Chemistry, 2002, 153, 211-219.	3.9	51
558	Enhanced and suppressed effects of ionic liquid on the photocatalytic activity of TiO2. Adsorption, 2013. 19. 557-561.	3.0	51

#	Article	IF	CITATIONS
559	Degradation of diclofenac by H2O2 activated with pre-magnetization Fe0: Influencing factors and degradation pathways. Chemosphere, 2018, 212, 853-862.	8.2	51
560	Preparation of Fluorine-Doped <mml:math xmlns:mml="http://www.w3.org/1998/Math/MathML"&gt;<mml:mrow><mml:msub><mml:mrow><mml:mtext>TiO mathvariant="bold"&gt;<mml:mrow><mml:mtext>2</mml:mtext></mml:mrow>with Controlled Crystalline Structure. International Journal of Photoenergy, 2008, 2008, 1-9.</mml:mtext></mml:mrow></mml:msub></mml:mrow></mml:math 		
561	Facile synthesis of porous Bi <sub>2</sub> WO <sub>6</sub> nanosheets with high photocatalytic performance. Dalton Transactions, 2015, 44, 14532-14539.	3.3	50
562	Organic Pollutant Photodecomposition by Ag/KNbO <sub>3</sub> Nanocomposites: A Combined Experimental and Theoretical Study. Journal of Physical Chemistry C, 2016, 120, 2777-2786.	3.1	50
563	Semiconductor Gas Sensor for Triethylamine Detection. Small, 2022, 18, e2104984.	10.0	50
564	Imperfect oriented attachment: Direct activation of high-temperature ferromagnetism in diluted magnetic semiconductor nanocrystals. Applied Physics Letters, 2006, 88, 223108.	3.3	49
565	Effect of structure-directing agents on facile hydrothermal preparation of hierarchical γ-Al2O3 and their adsorption performance toward Cr(VI) and CO2. Journal of Colloid and Interface Science, 2013, 401, 34-39.	9.4	49
566	EDTA, oxalate, and phosphate ions enhanced reactive oxygen species generation and sulfamethazine removal by zero-valent iron. Journal of Hazardous Materials, 2020, 391, 122210.	12.4	49
567	Dual-dehydrogenation-promoted catalytic oxidation of formaldehyde on alkali-treated Pt clusters at room temperature. Journal of Materials Chemistry A, 2015, 3, 10432-10438.	10.3	48
568	Photocatalytic NOx oxidation over modified ZnO/TiO2 thin films. Catalysis Today, 2015, 252, 41-46.	4.4	48
569	Hierarchical TiO <sub>2</sub> Submicrorods Improve the Photovoltaic Performance of Dye-Sensitized Solar Cells. ACS Sustainable Chemistry and Engineering, 2017, 5, 1315-1321.	6.7	48
570	Simultaneous removal of tetracycline and disinfection by a flow-through electro-peroxone process for reclamation from municipal secondary effluent. Journal of Hazardous Materials, 2019, 368, 771-777.	12.4	48
571	Enhancement of hydrogen peroxide production by electrochemical reduction of oxygen on carbon nanotubes modified with fluorine. Chemosphere, 2020, 259, 127423.	8.2	48
572	Electro-Fenton and photoelectro-Fenton degradation of sulfamethazine using an active gas diffusion electrode without aeration. Chemosphere, 2020, 250, 126177.	8.2	48
573	Facile preparation of monodispersed calcium carbonate spherical particles via a simple precipitation reaction. Materials Chemistry and Physics, 2004, 88, 1-4.	4.0	47
574	Fabrication of CdMoO <sub>4</sub> @CdS core–shell hollow superstructures as high performance visible-light driven photocatalysts. Physical Chemistry Chemical Physics, 2015, 17, 15339-15347.	2.8	47
575	Photoelectrochemical degradation of 2,4-dichlorophenoxyacetic acid using electrochemically self-doped Blue TiO2 nanotube arrays with formic acid as electrolyte. Journal of Hazardous Materials, 2020, 382, 121096.	12.4	47
576	Efficient H2O2 generation and spontaneous OH conversion for in-situ phenol degradation on nitrogen-doped graphene: Pyrolysis temperature regulation and catalyst regeneration mechanism. Journal of Hazardous Materials, 2020, 397, 122681.	12.4	47

#	Article	IF	CITATIONS
577	An <i>in situ</i> assembled WO <sub>3</sub> –TiO <sub>2</sub> vertical heterojunction for enhanced Z-scheme photocatalytic activity. Nanoscale, 2020, 12, 8775-8784.	5.6	47
578	C <sub>3</sub> N <sub>4</sub> /PDA S‣cheme Heterojunction with Enhanced Photocatalytic H <sub>2</sub> O <sub>2</sub> Production Performance and Its Mechanism. Advanced Sustainable Systems, 2023, 7, .	5.3	47
579	UV-resistant superhydrophobic BiOCl nanoflake film by a room-temperature hydrolysis process. Dalton Transactions, 2011, 40, 6632.	3.3	46
580	Facile synthesis of alumina hollow microspheres via trisodium citrate-mediated hydrothermal process and their adsorption performances for p-nitrophenol from aqueous solutions. Journal of Colloid and Interface Science, 2013, 394, 509-514.	9.4	46
581	Electrospun TiO <sub>2</sub> â€Based Photocatalysts. Solar Rrl, 2021, 5, 2000571.	5.8	46
582	Modulating the Electronic Metal‧upport Interactions in Singleâ€Atom Pt <sub>1</sub> â^'CuO Catalyst for Boosting Acetone Oxidation. Angewandte Chemie - International Edition, 2022, 61, .	13.8	46
583	Morphological control of calcium oxalate particles in the presence of poly-(styrene-alt-maleic acid). Journal of Solid State Chemistry, 2004, 177, 3368-3374.	2.9	45
584	Electrochemical properties of TiO2 hollow microspheres from a template-free and green wet-chemical route. Journal of Power Sources, 2008, 180, 869-874.	7.8	45
585	Different surfactants-assisted hydrothermal synthesis of hierarchical γ-Al2O3 and its adsorption performances for parachlorophenol. Chemical Engineering Journal, 2013, 233, 168-175.	12.7	45
586	Synthesis and photocatalytic activity of plasmonic Ag@AgCl composite immobilized on titanate nanowire films. Catalysis Today, 2014, 224, 193-199.	4.4	45
587	Nanosheet-based printable perovskite solar cells. Solar Energy Materials and Solar Cells, 2017, 159, 518-525.	6.2	45
588	Graphdiyne: A Brilliant Hole Accumulator for Stable and Efficient Planar Perovskite Solar Cells. Small, 2020, 16, e1907290.	10.0	45
589	Effect of nonionic structure-directing agents on adsorption and structural properties of mesoporous alumina. Journal of Materials Chemistry, 2011, 21, 9066.	6.7	44
590	Copperâ€Đecorated Microsized Nanoporous Titanium Dioxide Photocatalysts for Carbon Dioxide Reduction by Water. ChemCatChem, 2017, 9, 3054-3062.	3.7	44
591	Enhanced photocatalytic activity and mechanism of CeO2 hollow spheres for tetracycline degradation. Rare Metals, 2021, 40, 2369-2380.	7.1	44
592	0D/2D CdS/ZnO composite with n-n heterojunction for efficient detection of triethylamine. Journal of Colloid and Interface Science, 2021, 600, 898-909.	9.4	44
593	Rugby-like anatase titania hollow nanoparticles with enhanced photocatalytic activity. CrystEngComm, 2011, 13, 7044.	2.6	43
594	Complete Decomposition of Formaldehyde at Room Temperature over a Platinumâ€Decorated Hierarchically Porous Electrospun Titania Nanofiber Mat. ChemCatChem, 2014, 6, 1983-1989.	3.7	43

#	Article	IF	CITATIONS
595	Flexible Mg–Al layered double hydroxide supported Pt on Al foil for use in room-temperature catalytic decomposition of formaldehyde. RSC Advances, 2016, 6, 34280-34287.	3.6	43
596	N-doped graphene framework supported nickel cobalt oxide as supercapacitor electrode with enhanced performance. Applied Surface Science, 2019, 484, 135-143.	6.1	43
597	Iron-carbon microelectrolysis for wastewater remediation: Preparation, performance and interaction mechanisms. Chemosphere, 2021, 278, 130483.	8.2	43
598	Core–Shell Structured C@SiO <sub>2</sub> Hollow Spheres Decorated with Nickel Nanoparticles as Anode Materials for Lithiumâ€lon Batteries. Small, 2021, 17, e2103673.	10.0	43
599	Controlled synthesis of crystalline calcium carbonate aggregates with unusual morphologies involving the phase transformation from amorphous calcium carbonate. Materials Research Bulletin, 2009, 44, 831-835.	5.2	42
600	Glycine-assisted hydrothermal synthesis and adsorption properties of crosslinked porous α-Fe2O3 nanomaterials for p-nitrophenol. Chemical Engineering Journal, 2012, 211-212, 153-160.	12.7	42
601	A facile one-pot cation-anion double hydrolysis approach to the synthesis of supported MgO/γ-Al2O3 with enhanced adsorption performance towards CO2. Chemical Engineering Journal, 2017, 310, 216-225.	12.7	42
602	Lowâ€Temperatureâ€Processed Zr/F Coâ€Doped SnO <sub>2</sub> Electron Transport Layer for Highâ€Efficiency Planar Perovskite Solar Cells. Solar Rrl, 2020, 4, 2000090.	5.8	42
603	H2O molecule adsorption on s-triazine-based g-C3N4. Chinese Journal of Catalysis, 2021, 42, 115-122.	14.0	42
604	Photocatalytic TiO2/Glass Nanoflake Array Films. Langmuir, 2005, 21, 3486-3492.	3.5	41
605	Hydrothermal synthesis and photocatalytic activity of mesoporous titania hollow microspheres. Journal of Physics and Chemistry of Solids, 2008, 69, 1147-1151.	4.0	41
606	Chemistry of Trimethyl Aluminum: A Spontaneous Route to Thermally Stable 3D Crystalline Macroporous Alumina Foams with a Hierarchy of Pore Sizes. Chemistry of Materials, 2010, 22, 3251-3258.	6.7	41
607	Study of TiO2 anatase nano and microstructures with dominant {001} facets for NO oxidation. Environmental Science and Pollution Research, 2012, 19, 3719-3726.	5.3	41
608	Dependence of Exposed Facet of Pd on Photocatalytic H <sub>2</sub> -Production Activity. ACS Sustainable Chemistry and Engineering, 2018, 6, 6478-6487.	6.7	41
609	Trace FeCu@PC Derived from MOFs for Ultraefficient Heterogeneous Electro-Fenton Process: Enhanced Electron Transfer and Bimetallic Synergy. ACS ES&T Engineering, 2021, 1, 1311-1322.	7.6	41
610	S-doped MIL-53 as efficient heterogeneous electro-Fenton catalyst for degradation of sulfamethazine at circumneutral pH. Journal of Hazardous Materials, 2022, 424, 127674.	12.4	41
611	Large and ultrafast third-order optical nonlinearity of GeS2–Ga2S3–CdS chalcogenide glass. Chemical Physics Letters, 2004, 399, 230-233.	2.6	40
612	Ultrafine iron-cobalt nanoparticles embedded in nitrogen-doped porous carbon matrix for oxygen reduction reaction and zinc-air batteries. Journal of Colloid and Interface Science, 2019, 546, 113-121.	9.4	40

#	Article	IF	CITATIONS
613	Hierarchical NiMn <sub>2</sub> 0 <sub>4</sub> /rGO composite nanosheets decorated with Pt for low-temperature formaldehyde oxidation. Environmental Science: Nano, 2020, 7, 198-209.	4.3	40
614	One-pot template-free synthesis of porous CdMoO4 microspheres and their enhanced photocatalytic activity. Applied Surface Science, 2016, 387, 202-213.	6.1	39
615	Preparation of a Pt/TiO <sub>2</sub> /cotton fiber composite catalyst with low air resistance for efficient formaldehyde oxidation at room temperature. RSC Advances, 2017, 7, 21389-21397.	3.6	39
616	Preparation of transition metal composite graphite felt cathode for efficient heterogeneous electro-Fenton process. Environmental Science and Pollution Research, 2017, 24, 1122-1132.	5.3	39
617	Hole-conductor-free perovskite solar cells prepared with carbon counter electrode. Applied Surface Science, 2018, 430, 531-538.	6.1	39
618	Stable boron and cobalt co-doped TiO2 nanotubes anode for efficient degradation of organic pollutants. Journal of Hazardous Materials, 2020, 396, 122723.	12.4	39
619	Template-free solvothermal synthesis of hierarchical boehmite hollow microspheres with strong affinity toward organic pollutants in water. Materials Chemistry and Physics, 2013, 138, 167-173.	4.0	38
620	Cocatalyst modification and nanonization of Ag/AgCl photocatalyst with enhanced photocatalytic performance. Journal of Molecular Catalysis A, 2014, 381, 114-119.	4.8	38
621	Characterization of a novel strain phylogenetically related to Kocuria rhizophila and its chemical modification to improve performance of microbial fuel cells. Biosensors and Bioelectronics, 2015, 69, 113-120.	10.1	38
622	Efficient transformative HCHO capture by defective NH <sub>2</sub> -UiO-66(Zr) at room temperature. Environmental Science: Nano, 2019, 6, 2931-2936.	4.3	38
623	Nanocages of Polymeric Carbon Nitride from Low‶emperature Supramolecular Preorganization for Photocatalytic CO <sub>2</sub> Reduction. Solar Rrl, 2020, 4, 1900469.	5.8	38
624	A novel electro-Fenton process coupled with sulfite: Enhanced Fe3+ reduction and TOC removal. Journal of Hazardous Materials, 2022, 422, 126888.	12.4	38
625	Preparation and characterization of SiO2/TiO2 composite microspheres with microporous SiO2 core/mesoporous TiO2 shell. Journal of Solid State Chemistry, 2005, 178, 1818-1824.	2.9	37
626	DNA-mediated morphosynthesis of calcium carbonate particles. Journal of Colloid and Interface Science, 2010, 352, 43-49.	9.4	37
627	Electrochemically reduced graphene oxide on silicon nanowire arrays for enhanced photoelectrochemical hydrogen evolution. Dalton Transactions, 2016, 45, 13717-13725.	3.3	37
628	Fabrication of hierarchical bristle-grass-like NH4Al(OH)2CO3@Ni(OH)2 core-shell structure and its enhanced Congo red adsorption performance. Journal of Alloys and Compounds, 2018, 750, 644-654.	5.5	37
629	Hydrogen-bond activation of N2 molecules and photocatalytic nitrogen fixation. CheM, 2021, 7, 1983-1985.	11.7	37
630	Synergy between Platinum and Gold Nanoparticles in Oxygen Activation for Enhanced Roomâ€īemperature Formaldehyde Oxidation. Advanced Functional Materials, 2022, 32, .	14.9	37

#	Article	IF	CITATIONS
631	Shape evolution of SrCO3 particles in the presence of poly-(styrene-alt-maleic acid). Journal of Solid State Chemistry, 2006, 179, 800-803.	2.9	36
632	A comparative study of azo dye decolorization by electroâ€Fenton in two common electrolytes. Journal of Chemical Technology and Biotechnology, 2009, 84, 1544-1549.	3.2	36
633	Efficient decomposition of formaldehyde at room temperature over Pt/honeycomb ceramics with ultra-low Pt content. Dalton Transactions, 2014, 43, 12935.	3.3	36
634	Grapheneâ€Based Materials in Planar Perovskite Solar Cells. Solar Rrl, 2020, 4, 2000502.	5.8	36
635	Solar-Driven Glucose Isomerization into Fructose via Transient Lewis Acid–Base Active Sites. ACS Catalysis, 2021, 11, 12170-12178.	11.2	36
636	Effects of poly (sodium 4-styrene-sulfonate) on morphology of calcium carbonate particles. Journal of Crystal Growth, 2006, 294, 358-366.	1.5	35
637	Facile synthesis and enhanced visible-light photocatalytic activity of Ag2S nanocrystal-sensitized Ag8W4O16 nanorods. Journal of Colloid and Interface Science, 2014, 422, 30-37.	9.4	35
638	Role of adsorption and oxidation in porous carbon aerogel/persulfate system for non-radical degradation of organic contaminant. Chemosphere, 2020, 241, 125066.	8.2	35
639	Hierarchical Co3O4-NiO hollow dodecahedron-supported Pt for room-temperature catalytic formaldehyde decomposition. Chemical Engineering Journal, 2022, 430, 132715.	12.7	35
640	Effects of PSMA additive on morphology of barite particles. Journal of Crystal Growth, 2005, 275, 572-579.	1.5	34
641	Vapor-thermal preparation of highly crystallized TiO2 powder and its photocatalytic activity. Journal of Solid State Chemistry, 2007, 180, 2080-2087.	2.9	34
642	Greatly enhanced photocatalytic activity of TiO2â^'xNx by a simple surface modification of Fe(III) cocatalyst. Journal of Molecular Catalysis A, 2014, 391, 92-98.	4.8	34
643	Hollow carbon sphere-supported Pt/CoO hybrid with excellent hydrogen evolution activity and stability in acidic environment. Applied Catalysis B: Environmental, 2022, 314, 121503.	20.2	34
644	Influence of PSSS additive and temperature on morphology and phase structures of calcium oxalate. Journal of Colloid and Interface Science, 2005, 288, 407-411.	9.4	33
645	Preparation, characterization and photocatalytic activity of novel TiO2 nanoparticle-coated titanate nanorods. Journal of Molecular Catalysis A, 2006, 253, 99-106.	4.8	33
646	Poly(methacrylic acid)-mediated morphosynthesis of PbWO4 micro-crystals. Applied Physics A: Materials Science and Processing, 2007, 87, 113-120.	2.3	33
647	Synergistic effect of CoPi-hole and Cu( <scp>ii</scp> )-electron cocatalysts for enhanced photocatalytic activity and photoinduced stability of Ag <sub>3</sub> PO <sub>4</sub> . Physical Chemistry Chemical Physics, 2017, 19, 10309-10316.	2.8	33
648	Atomically thin two-dimensional ZnSe/ZnSe(ea) <sub>x</sub> van der Waals nanojunctions for synergistically enhanced visible light photocatalytic H <sub>2</sub> evolution. Nanoscale, 2019, 11, 17718-17724.	5.6	33

#	Article	IF	CITATIONS
649	DFT Study on Regulating the Electronic Structure and CO2 Reduction Reaction in BiOBr/Sulphur-Doped G-C3N4 S-Scheme Heterojunctions. Frontiers in Nanotechnology, 2021, 3, .	4.8	33
650	Generation of hydroxyl radicals by metal-free bifunctional electrocatalysts for enhanced organics removal. Science of the Total Environment, 2021, 791, 148107.	8.0	33
651	In situ Monitoring of Heterogeneous Catalytic Reactions. ChemPhysChem, 2010, 11, 1617-1618.	2.1	32
652	Rapid synthesis of a TiO2 hollow microsphere assembly from hollow nanoparticles with enhanced photocatalytic activity. RSC Advances, 2013, 3, 15273.	3.6	32
653	Template-free synthesis of hierarchical $\hat{1}^3$ -Al <sub>2</sub> O <sub>3</sub> nanostructures and their adsorption affinity toward phenol and CO <sub>2</sub> . RSC Advances, 2015, 5, 7066-7073.	3.6	31
654	Pre-magnetized Fe0 as heterogeneous electro-Fenton catalyst for the degradation of p-nitrophenol at neutral pH. Chemosphere, 2020, 240, 124962.	8.2	31
655	Triethanolamine-assisted photodeposition of non-crystalline Cu <sub>x</sub> P nanodots for boosting photocatalytic H <sub>2</sub> evolution of TiO <sub>2</sub> . Journal of Materials Chemistry C, 2020, 8, 15816-15822.	5.5	31
656	Kinetic and mechanism study of UV/pre-magnetized-Fe0/oxalate for removing sulfamethazine. Journal of Hazardous Materials, 2020, 398, 122931.	12.4	31
657	A Blinking Mesoporous TiO <sub>2â~'<i>x</i></sub> Composed of Nanosized Anatase with Unusually Longâ€Lived Trapped Charge Carriers. Angewandte Chemie - International Edition, 2020, 59, 15000-15007.	13.8	31
658	Structural investigations of GeS2–Ga2S3–CdS chalcogenide glasses using Raman spectroscopy. Solid State Communications, 2004, 130, 459-464.	1.9	30
659	Efficient removal of gaseous formaldehyde in air using hierarchical titanate nanospheres with in situ amine functionalization. Physical Chemistry Chemical Physics, 2016, 18, 18161-18168.	2.8	30
660	Engineering 2D NiO/Ni3S2 heterointerface electrocatalyst for highly efficient hydrogen production coupled with benzyl alcohol oxidation. Chemical Engineering Journal, 2022, 431, 134137.	12.7	30
661	Graphdiyne-based photocatalysts for solar fuel production. Green Chemistry, 2022, 24, 5739-5754.	9.0	30
662	Atomic Force Microscopic Studies of Porous TiO2 Thin Films Prepared by the Sol-Gel Method. Journal of Sol-Gel Science and Technology, 2002, 24, 229-240.	2.4	29
663	Synthesis of BaWO4 Hollow Structures. Crystal Growth and Design, 2006, 6, 2210-2213.	3.0	29
664	Preparation of monodispersed microporous SiO2 microspheres with high specific surface area using dodecylamine as a hydrolysis catalyst. Journal of Solid State Chemistry, 2006, 179, 226-232.	2.9	29
665	A novel solid-state electrochemiluminescence sensor based on Ru(bpy)32 +immobilization on TiO2nanotube arrays and its application for detection of amines in water. Nanotechnology, 2010, 21, 245501.	2.6	29
666	A highly efficient flow-through electro-Fenton system enhanced with nitrilotriacetic acid for phenol removal at neutral pH. Science of the Total Environment, 2019, 697, 134173.	8.0	29

#	Article	IF	CITATIONS
667	Ultra-Thin Carbon-Doped Bi2WO6 Nanosheets for Enhanced Photocatalytic CO2 Reduction. Transactions of Tianjin University, 2021, 27, 338-347.	6.4	29
668	Effects of urea on the microstructure and photocatalytic activity of bimodal mesoporous titania microspheres. Journal of Molecular Catalysis A, 2009, 313, 107-113.	4.8	28
669	Enhancement of Visible-Light Photocatalytic Activity of Mesoporous Au-TiO <sub>2</sub> Nanocomposites by Surface Plasmon Resonance. International Journal of Photoenergy, 2012, 2012, 1-10.	2.5	28
670	Simultaneous electricity generation and tetracycline removal in continuous flow electrosorption driven by microbial fuel cells. RSC Advances, 2015, 5, 49513-49520.	3.6	28
671	Mechanistic Insight into the Heterogeneous Electro-Fenton/Sulfite Process for Ultraefficient Degradation of Pollutants over a Wide pH Range. ACS ES&T Water, 2021, 1, 1637-1647.	4.6	28
672	Thermal and optical properties of GeS2-based chalcogenide glasses. Materials Science and Engineering B: Solid-State Materials for Advanced Technology, 2004, 110, 38-41.	3.5	27
673	Solvothermal synthesis of novel dendrite-like SnS particles in a mixed solvent of ethylenediamine and dodecanethiol. Journal of Alloys and Compounds, 2008, 460, 513-518.	5.5	27
674	Characterization and visible light photocatalytic properties of nanocrystalline TiO2 synthesized by reactive plasma processing. Solar Energy Materials and Solar Cells, 2009, 93, 1540-1549.	6.2	27
675	Fe3O4 nanoparticles as an efficient heterogeneous Fenton catalyst for phenol removal at relatively wide pH values. Water Science and Technology, 2013, 68, 2367-2373.	2.5	27
676	Design of highly-active photocatalytic materials for solar fuel production. Chemical Engineering Journal, 2021, 421, 127732.	12.7	27
677	Highly dispersed MoS <sub>x</sub> nanodot-modified TiO <sub>2</sub> photocatalysts: vitamin C-mediated synthesis and improved H <sub>2</sub> evolution activity. Journal of Materials Chemistry C, 2021, 9, 3239-3246.	5.5	27
678	Facile preparation of Na-free anatase TiO2 film with highly photocatalytic activity on soda-lime glass. Catalysis Communications, 2006, 7, 1000-1004.	3.3	26
679	Enhancement of bioelectricity generation via heterologous expression of IrrE in Pseudomonas aeruginosa-inoculated MFCs. Biosensors and Bioelectronics, 2018, 117, 23-31.	10.1	26
680	Low-temperature fabrication and photocatalytic activity of clustered TiO2 particles formed on glass fibers. Journal of Crystal Growth, 2005, 280, 612-619.	1.5	25
681	Building dual active sites Co3O4/Cu electrode to break scaling relations for enhancement of electrochemical reduction of nitrate to high-value ammonia. Journal of Hazardous Materials, 2022, 434, 128887.	12.4	25
682	Cadmium Chalcogenide (CdS, CdSe, CdTe) Quantum Dots for Solarâ€ŧoâ€Fuel Conversion. Advanced Photonics Research, 2022, 3, .	3.6	25
683	Formation and properties of chalcogenide glasses in the GeS2–Ga2S3–CdS system. Materials Chemistry and Physics, 2004, 83, 284-288.	4.0	24
684	Effect of a new functional double-hydrophilic block copolymer PAAL on the morphology of calcium carbonate particles. Materials Research Bulletin, 2005, 40, 656-664.	5.2	24

#	Article	IF	CITATIONS
685	Influence of PSSS on the morphology and polymorph of calcium carbonate in the ethanol–water mixed system. Journal of Alloys and Compounds, 2008, 463, 343-349.	5.5	24
686	The role of electron interfacial transfer in mesoporous nano-TiO <sub>2</sub> photocatalysis: a combined study of in situ photoconductivity and numerical kinetic simulation. Physical Chemistry Chemical Physics, 2017, 19, 8866-8873.	2.8	24
687	In-situ synthesis of amorphous H2TiO3-modified TiO2 and its improved photocatalytic H2-evolution performance. Journal of Colloid and Interface Science, 2018, 532, 272-279.	9.4	24
688	Principle and surface science of photocatalysis. Interface Science and Technology, 2020, 31, 1-38.	3.3	24
689	Preparation and photocatalytic activity of multi-modally macro/mesoporous titania. Research on Chemical Intermediates, 2009, 35, 653-665.	2.7	23
690	In Situ Transformation of Prussianâ€Blue Analogueâ€Derived Bimetallic Carbide Nanocubes by Water Oxidation: Applications for Energy Storage and Conversion. Chemistry - A European Journal, 2020, 26, 4052-4062.	3.3	23
691	Ultrathin 2D/2D Graphdiyne/Bi <sub>2</sub> WO <sub>6</sub> Heterojunction for Gas-Phase CO <sub>2</sub> Photoreduction. ACS Applied Energy Materials, 2021, 4, 8734-8738.	5.1	23
692	Fabrication, characterization and photocatalytic activity of preferentially oriented TiO2 films. Journal of Crystal Growth, 2006, 295, 60-68.	1.5	22
693	Amorphous Ti( <scp>iv</scp> )-modified Bi <sub>2</sub> WO <sub>6</sub> with enhanced photocatalytic performance. RSC Advances, 2016, 6, 65902-65910.	3.6	22
694	Enhancement of CO2 biofixation and bioenergy generation using a novel airlift type photosynthetic microbial fuel cell. Bioresource Technology, 2019, 272, 501-509.	9.6	22
695	Activated Carbon Derived from Rice Husk as Efficient Oxygen Reduction Catalyst in Microbial Fuel Cell. Electroanalysis, 2020, 32, 2969-2975.	2.9	22
696	Selenium-Rich Configuration and Amorphization for Synergistically Maximizing the Active-Center Amount of CoSe <sub>1+<i>x</i></sub> Nanodots toward Efficient Photocatalytic H <sub>2</sub> Evolution. ACS Sustainable Chemistry and Engineering, 2021, 9, 8653-8662.	6.7	22
697	ZIF-8 derived ZnO-CsPbBr3 polyhedrons for efficient triethylamine detection. Sensors and Actuators B: Chemical, 2022, 357, 131366.	7.8	22
698	Facile fabrication of SiO2/Al2O3 composite microspheres with a simple electrostatic attraction strategy. Materials Research Bulletin, 2008, 43, 714-722.	5.2	21
699	Microbial fuel cells and microbial electrolysis cells for the production of bioelectricity and biomaterials. Environmental Technology (United Kingdom), 2013, 34, 1915-1928.	2.2	21
700	A first preâ€pilot system for the combined treatment of dye pollutants by electrocoagulation/ <scp>EAOPs</scp> . Journal of Chemical Technology and Biotechnology, 2014, 89, 1136-1144.	3.2	21
701	Hierarchically macro–mesoporous TiO2 film via self-assembled strategy for enhanced efficiency of dye sensitized solar cells. Materials Research Bulletin, 2016, 74, 380-386.	5.2	21
702	Facile preparation of monodispersed SiO2/TiO2 composite microspheres with high surface area. Materials Chemistry and Physics, 2006, 96, 311-316.	4.0	20

#	Article	IF	CITATIONS
703	Low-temperature hydrothermal synthesis of highly photoactive mesoporous spherical TiO2 nanocrystalline. Journal of Physics and Chemistry of Solids, 2010, 71, 507-510.	4.0	20
704	Kinetic study of the degradation of rhodamine B using a flow-through UV/electro-Fenton process with the presence of ethylenediaminetetraacetic acid. Chemosphere, 2020, 240, 124929.	8.2	20
705	Metal–organic framework with atomically dispersed Ni–N4 sites for greatly-raised visible-light photocatalytic H2 production. Chemical Engineering Journal, 2022, 431, 133944.	12.7	20
706	Facile fabrication of monodispersed mesoporous celestine particles with peanut-shaped morphology. Journal of Crystal Growth, 2005, 279, 461-465.	1.5	19
707	Facile preparation, characterization and optical properties of rectangular PbCrO4 single-crystal nanorods. Journal of Alloys and Compounds, 2007, 431, L4-L7.	5.5	19
708	Solvothermal synthesis and photocatalytic performance of Mg2+-doped anatase nanocrystals with exposed {001} facets. Catalysis Today, 2014, 230, 125-130.	4.4	19
709	Hydrothermal Synthesis of Modified Hydrophobic Zn–Al-Layered Double Hydroxides Using Structure-Directing Agents and Their Enhanced Adsorption Capacity for <i>p</i> -Nitrophenol. Adsorption Science and Technology, 2014, 32, 351-364.	3.2	19
710	Sulfideâ€Based Nickelâ€Plated Fabrics for Foldable Quasiâ€5olidâ€5tate Supercapacitors. Energy and Environmental Materials, 2022, 5, 883-891.	12.8	19
711	Fewâ€Layered Mo <sub><i>x</i></sub> W <sub>1â^'<i>x</i></sub> S <sub>2</sub> â€Modified CdS Photocatalyst: Oneâ€Step Synthesis with Bifunctional Precursors and Improved H <sub>2</sub> â€Evolution Activity. Solar Rrl, 2021, 5, 2100387.	5.8	19
712	Nickelâ€ʿcobalt selenide@N-doped carbon towards high-performance anode materials for sodium-ion batteries. Journal of Energy Storage, 2022, 51, 104522.	8.1	19
713	The radical and non-radical oxidation mechanism of electrochemically activated persulfate process on different cathodes in divided and undivided cell. Journal of Hazardous Materials, 2021, 416, 125804.	12.4	18
714	Potassium/oxygen co-doped polymeric carbon nitride for enhanced photocatalytic CO2 reduction. Applied Surface Science, 2021, 563, 150310.	6.1	18
715	Enhanced performance of CH3NH3PbI3 perovskite solar cells by excess halide modification. Applied Surface Science, 2021, 564, 150464.	6.1	18
716	Surface and interface modification strategies of CdS-based photocatalysts. Interface Science and Technology, 2020, , 313-348.	3.3	17
717	Degradation of 2,4-dichlorophenoxyacetic acid by a novel photoelectrocatalysis/photoelectro-Fenton process using Blue-TiO2 nanotube arrays as the anode. Chemosphere, 2021, 266, 129063.	8.2	17
718	Electron-enriched regulation of sulfur-active site for accelerating atomic hydrogen desorption of S-rich MoWS2+ cocatalyst toward efficient photocatalytic H2 evolution of TiO2. Chemical Engineering Journal, 2022, 449, 137803.	12.7	17
719	Preparation and characterization of highly photoactive nanocrystalline TiO2 powders by solvent evaporation-induced crystallization method. Science in China Series B: Chemistry, 2003, 46, 549.	0.8	16
720	Influence of solvation interactions on the zeta potential of titania powders. Journal of Colloid and Interface Science, 2003, 262, 97-100.	9.4	16

#	Article	IF	CITATIONS
721	Large-scale in situ synthesis and characterization of ternary single-crystal NaV6O15 nanoneedles. Materials Chemistry and Physics, 2007, 104, 362-366.	4.0	16
722	A cost-effective polyurethane based activated carbon sponge anode for high-performance microbial fuel cells. RSC Advances, 2015, 5, 84269-84275.	3.6	16
723	From Millimeter to Subnanometer: Vapor–Solid Deposition of Carbon Nitride Hierarchical Nanostructures Directed by Supramolecular Assembly. Angewandte Chemie, 2017, 129, 8546-8550.	2.0	16
724	MnCo Oxides Supported on Carbon Fibers for High-Performance Supercapacitors. Wuli Huaxue Xuebao/ Acta Physico - Chimica Sinica, 2020, 36, 1907072-0.	4.9	16
725	A novel approach for the synthesis of monodispersed porous silica microspheres with high surface area. Journal of Non-Crystalline Solids, 2005, 351, 3593-3599.	3.1	15
726	Polymer-directed large-scale synthesis of single-crystal vanadium oxide nanobelts. Materials Chemistry and Physics, 2006, 95, 206-210.	4.0	15
727	Solvothermal synthesis of novel flower-like manganese sulfide particles. Journal of Physics and Chemistry of Solids, 2008, 69, 1342-1345.	4.0	15
728	Adsorption equilibrium and kinetic study of guaifenesin enantiomers on cellulose tris 3,5-dimethylphenylcarbamate packed column. Chemical Engineering Journal, 2014, 244, 128-136.	12.7	15
729	Hydroxyl-enriched highly crystalline TiO <sub>2</sub> suspensible photocatalyst: facile synthesis and superior H <sub>2</sub> -generation activity. Chemical Communications, 2021, 57, 2025-2028.	4.1	15
730	WO <sub>3</sub> Nanosheet-Supported IrW Alloy for High-Performance Acidic Overall Water Splitting with Low Ir Loading. ACS Applied Energy Materials, 2022, 5, 970-980.	5.1	15
731	Aminopolycarboxylic acids modified oxygen reduction by zero valent iron: Proton-coupled electron transfer, role of iron ion and reactive oxidant generation. Journal of Hazardous Materials, 2022, 430, 128402.	12.4	15
732	A stochastic study of electron transfer kinetics in nano-particulate photocatalysis: a comparison of the quasi-equilibrium approximation with a random walking model. Physical Chemistry Chemical Physics, 2016, 18, 31914-31923.	2.8	14
733	Amorphous WO <sub>3</sub> induced lattice distortion for a low-cost and high-efficient electrocatalyst for overall water splitting in acid. Sustainable Energy and Fuels, 2020, 4, 1712-1722.	4.9	14
734	Designing a 0D/2D Sâ€5cheme Heterojunction over Polymeric Carbon Nitride for Visibleâ€Light Photocatalytic Inactivation of Bacteria. Angewandte Chemie, 2020, 132, 5256-5263.	2.0	14
735	A 3D Hierarchical Ti <sub>3</sub> C <sub>2</sub> T <sub>x</sub> /TiO <sub>2</sub> Heterojunction for Enhanced Photocatalytic CO <sub>2</sub> Reduction. ChemNanoMat, 2021, 7, 910-915.	2.8	14
736	A continuous flow-through system with integration of electrosorption and peroxi-coagulation for efficient removal of organics. Chemosphere, 2021, 274, 129983.	8.2	14
737	A Comparative Study of Cobalt Chalcogenides as the Electrode Materials on Lithium‣ulfur Battery Performance. Small Methods, 2022, 6, e2101269.	8.6	14
738	Donor–Acceptor Modification of Carbon Nitride for Enhanced Photocatalytic Hydrogen Evolution. Advanced Sustainable Systems, 2023, 7, .	5.3	14

#	Article	IF	CITATIONS
739	Title is missing!. Journal of Materials Science Letters, 2001, 20, 671-673.	0.5	13
740	Effects of polyvinylpyrrolidone and cetyltrimethylammonium bromide on morphology of lead tungstate particles. Journal of Alloys and Compounds, 2007, 433, 73-78.	5.5	13
741	Morphology control of copper oxalate polycrystalline particles involving an etching process. Journal of Crystal Growth, 2007, 306, 366-372.	1.5	13
742	Significant capacitance enhancement induced by cyclic voltammetry in pine needle-like Ni-Co-Cu multicomponent electrode. Journal of Materials Science and Technology, 2021, 78, 100-109.	10.7	13
743	Global regulator engineering enhances bioelectricity generation in Pseudomonas aeruginosa-inoculated MFCs. Biosensors and Bioelectronics, 2020, 163, 112269.	10.1	13
744	Morphological control of strontium oxalate particles by PSMA-mediated precipitation reaction. Materials Chemistry and Physics, 2005, 91, 134-139.	4.0	12
745	Facile synthesis of monodispersed barium sulphate particles via an in situ templated process. Journal of Colloid and Interface Science, 2007, 311, 89-93.	9.4	12
746	Synthesis, Characterization, Properties, and Applications of Nanosized Photocatalytic Materials. Journal of Nanomaterials, 2012, 2012, 1-3.	2.7	12
747	Architectural design of hierarchically meso–macroporous carbon for microbial fuel cell anodes. RSC Advances, 2016, 6, 27993-27998.	3.6	12
748	Design and fabrication of direct Z-scheme photocatalysts. Interface Science and Technology, 2020, 31, 193-229.	3.3	12
749	Enhanced degradation of 2,4-dichlorophenoxyacetic acid by electro-fenton in flow-through system using B, Co-TNT anode. Chemosphere, 2022, 292, 133470.	8.2	12
750	Effects of PSMA and experimental conditions on the morphologies of BaCO3 whiskers. Rare Metals, 2006, 25, 382-388.	7.1	11
751	Energy and environmental photocatalytic materials. Applied Surface Science, 2017, 391, 71.	6.1	11
752	Effects of Ti precursors on the performance of planar perovskite solar cells. Applied Surface Science, 2018, 462, 598-605.	6.1	11
753	Modification of ZnO-based photocatalysts for enhanced photocatalytic activity. Interface Science and Technology, 2020, , 265-284.	3.3	11
754	Cu <sub>2</sub> O-rGO-CuO Composite: An Effective Z-scheme Visible-Light Photocatalyst. Current Nanoscience, 2015, 11, 462-469.	1.2	11
755	CO2 capture and in situ photocatalytic reduction. Chem Catalysis, 2022, 2, 428-430.	6.1	11
756	Controlled Synthesis of Novel Flower-shaped BaCrO4Crystals. Chemistry Letters, 2005, 34, 564-565.	1.3	10

#	Article	IF	CITATIONS
757	Crystallization of lead sulfide in the presence of poly(methacrylic acid) or/and cetyltrimethylammonium bromide. Colloids and Surfaces A: Physicochemical and Engineering Aspects, 2005, 268, 78-84.	4.7	10
758	Photocatalytic Materials. International Journal of Photoenergy, 2012, 2012, 1-5.	2.5	10
759	Influence of calcination temperature on photocatalytic H <sub>2</sub> O <sub>2</sub> productivity of hierarchical porous ZnO microspheres. Nanotechnology, 2021, 32, 415402.	2.6	10
760	Fabrication of Ru(bpy)32+-titanate nanotube nanocomposite and its application as sensitive solid-state electrochemiluminescence sensor material. Journal of Physics and Chemistry of Solids, 2010, 71, 527-529.	4.0	9
761	A figure of merits-based performance comparison of various advanced functional nanomaterials for adsorptive removal of gaseous ammonia. Science of the Total Environment, 2022, 822, 153428.	8.0	9
762	Facile Preparation of Strontium Tungstate and Tungsten Trioxide Hollow Spheres. Journal of the American Ceramic Society, 2006, 89, 060623005134010-???.	3.8	8
763	Morphology control of lead sulfide particles in mixed systems of poly-(styrene-alt-maleic acid) and cetyltrimethylammonium bromide. Materials Chemistry and Physics, 2007, 101, 379-382.	4.0	8
764	Synthesis of BaMoO4 hollow spheres. Journal of Materials Science, 2007, 42, 6716.	3.7	8
765	Cost-effective copper removal by electrosorption powered by microbial fuel cells. Bioprocess and Biosystems Engineering, 2016, 39, 511-519.	3.4	8
766	Degradation of Diclofenac Sodium by Pre-magnetization Fe0/Persulfate System: Efficiency and Degradation Pathway Study. Water, Air, and Soil Pollution, 2020, 231, 1.	2.4	8
767	New progress on MXenes-based nanocomposite photocatalysts. Materials Reports Energy, 2022, 2, 100081.	3.2	7
768	Controlled synthesis of semiconductor PbWO4 nanocrystals inside silica SBA-15 materials. Advanced Powder Technology, 2011, 22, 576-580.	4.1	6
769	Enhanced Electrochemiluminescence Performance of Ru(bpy) <sub>3</sub> <sup>2+</sup> /CuO/TiO <sub>2</sub> Nanotube Array Sensor for Detection of Amines. Electroanalysis, 2014, 26, 2017-2022.	2.9	6
770	Enhancing photocatalytic activity of the sol-gel derived TiO2 thin films by nitric acid treatment. Journal of Materials Science Letters, 2003, 22, 967-970.	0.5	5
771	Amperometric Determination of Chemical Oxygen Demand via the Functional Combination of Three Digestion Types. Electroanalysis, 2010, 22, 2947-2959.	2.9	5
772	In-Flight Formation of Nano-Crystalline Titanium Dioxide Powder in a Plasma Jet and Its Characterization. Plasma Science and Technology, 2010, 12, 426-432.	1.5	5
773	Environmental Photocatalysis. International Journal of Photoenergy, 2012, 2012, 1-4.	2.5	5
774	Emerging Solar Photocatalysis. Solar Rrl, 2021, 5, 2100252.	5.8	5

#	Article	IF	CITATIONS
775	Enhanced electricity generation and tetracycline removal of bioelectro-Fenton with electroactive biofilm induced by multi external resistance. Chemosphere, 2022, 289, 133070.	8.2	5
776	Preparation and formation mechanism of wood-block-like calcite particles. Journal of Solid State Chemistry, 2006, 179, 2547-2553.	2.9	4
777	Creation of calcite hollow microspheres with attached bundles of aragonite needles. Crystal Research and Technology, 2008, 43, 473-478.	1.3	4
778	Facile Preparation and Photoinduced Superhydrophilicity of Highly Ordered Sodium-Free Titanate Nanotube Films by Electrophoretic Deposition. International Journal of Photoenergy, 2012, 2012, 1-6.	2.5	4
779	Environmental Photocatalysis 2013. International Journal of Photoenergy, 2013, 2013, 1-3.	2.5	4
780	Hierarchical porous photocatalysts. Interface Science and Technology, 2020, , 63-102.	3.3	4
781	Surface heterojunction of photocatalysts. Interface Science and Technology, 2020, 31, 161-191.	3.3	4
782	Agl-BiOI Spherical Solid Solutions with Enhanced Visible-Light Photocatalytic Performances. Current Nanoscience, 2015, 11, 453-461.	1.2	4
783	A Blinking Mesoporous TiO <sub>2â^'<i>x</i></sub> Composed of Nanosized Anatase with Unusually Longâ€Lived Trapped Charge Carriers. Angewandte Chemie, 2020, 132, 15110-15117.	2.0	4
784	Modulating the Electronic Metalâ€Support Interactions in Singleâ€Atom Pt <sub>1</sub> â^'CuO Catalyst for Boosting Acetone Oxidation. Angewandte Chemie, 2022, 134, .	2.0	4
785	Effects of microwave drying on the microstructure and photocatalytic activity of bimodal mesoporous TiO2 powders. Journal of Physics and Chemistry of Solids, 2010, 71, 523-526.	4.0	3
786	Effect of F-Doping on the Photocatalytic Activity and Microstructures of Nanocrystalline TiO2 Powders. Nanostructure Science and Technology, 2016, , 187-200.	0.1	3
787	TiO2Photocatalytic Materials 2013. International Journal of Photoenergy, 2013, 2013, 1-2.	2.5	2
788	Water Splitting By Photocatalytic Reduction. Green Chemistry and Sustainable Technology, 2016, , 175-210.	0.7	2
789	Surface modification of g-C3N4: first-principles study. Interface Science and Technology, 2020, 31, 509-539.	3.3	2
790	Photocatalysts based on polymeric carbon nitride for solar-to-fuel conversion. Interface Science and Technology, 2020, 31, 475-507.	3.3	2
791	Hydrazine hydrate chemical reduction as an effective anode modification method to improve the performance of microbial fuel cells. Journal of Chemical Technology and Biotechnology, 2013, 88, 2075-2081.	3.2	1
792	2nd international workshop on graphene and C 3 N 4 -based photocatalysts. Applied Surface Science, 2018, 430, 1.	6.1	1

#	Article	IF	CITATIONS
793	Graphene oxide-based photocatalysts for H2 production. , 2022, , 65-92.		1
794	Nanosized Photocatalytic Materials 2013. Journal of Nanomaterials, 2014, 2014, 1-2.	2.7	0
795	TiO <sub>2</sub> Photocatalytic Materials 2014. International Journal of Photoenergy, 2015, 2015, 1-2.	2.5	0
796	Solar Fuel Photocatalysts. , 2015, , .		0
797	Introductory chapter: Fundamentals of photocatalysis and electrocatalysis. , 2022, , 1-30.		0
798	Graphene oxide-based modified electrodes for high-performance supercapacitors. , 2022, , 239-266.		0
799	Graphene oxide-based photocatalysts for environmental purification. , 2022, , 135-172.		0
800	Graphene oxide-based heterojunction photocatalysts. , 2022, , 173-188.		0
801	Graphene oxide-based photocatalysts for CO2 reduction. , 2022, , 93-134.		0
802	Graphene oxide-based materials in electrocatalysis. , 2022, , 189-238.		0